Contents — T through Z

Locations and compositions of mare ponds in South pole-Aitken basin on the moon and its implication to the impact tectonics. T. Takata and S. Hori, Miyagi University of Education (Aoba, Sendai, 980-0845 JAPAN, toshiko@miyakyo-u.ac.jp).

ABSTRACT: Locations and compositions of mare ponds in South pole-Aitken (SPA) basin are correlated to the structure of the SPA impact basin. The coverage of mare emplacements indicates that, inside the inner ring, the floor is relatively filled with mare deposits, whereas, in the regions of just inside the middle and outer rings, some mare extrusions exist. The lack of Hi-Ti basalt in mare ponds could result from the subsurface structure of the SPA post impact.

Introduction: Most of volcanic activities were taken place in impact basins on the moon. The structure of impact basins is a key to the development of the magma chamber in the lunar mantle and the extrusion of the magma to the lunar surface. On the farside of the moon, the large impact basin –South pole-Aitken (SPA) exists, and mare ponds are well discrete to locate their eruptive sites relative to the impact basin. In order to examine the correlation of the impact tectonics of the SPA cratering and volcanic activities, locations and compositions of mare ponds are related to the SPA impact structure.

Distribution of Mare ponds:

Methods: The area coverage of mare ponds becomes an index of the eruptive activities. The coverage is estimated as a function of the radial distance from the center of the SPA crater (180 ° E, 50 ° S) using the estimate of locations and extended area of mare ponds [1]. The SPA is divided into several concentric circles with a radial distance of 4 degrees (approximately 120 *km/bin*). The total area of mare ponds in each bin is divided by the area of the bin, and then the coverage of the mare deposits is calculated.

Results: Figure 1 shows the highest coverage in the SPA central region (<20degree ~ radial distance of 630 km) and small peaks near ring regions. A similar tendency is observed in the Orientale basin [2]. In the inner ring, crater floor is rather filled with volcanic emplacements, whereas, some mare extrusions were emplaced in regions just inside the middle and outer rings. This implicates that volcanic dikes from the lunar mantle could easily reach the surface inside and along rings. Tectonic normal faulting systems of middle and outer rings could assist the extrusion of magma to the surface. Inside the inner ring, the shallow-seated magma chambers could be erupted due to the lack of excavated crust excavated crust materials, brecciated deposits and lower-pressurized subsurface materials in the center of impact. Thus, the structure of the crater is possibly related to the inductions of volcanic emplacements. The depth of these faulting roots and magma source can be derived from the compositional analysis. Thus, in next, Clementine UVVIS data is utilized for further compositional analysis of mare deposits.

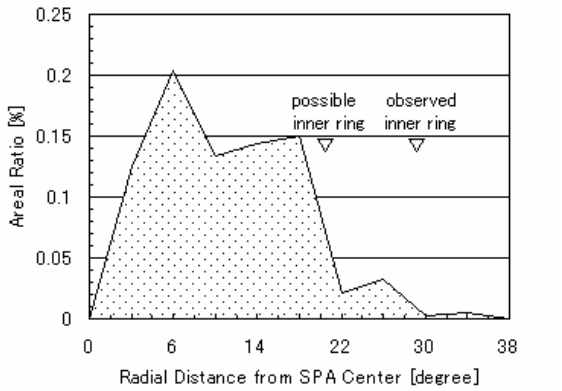

Figure 1. Area ratio of mare ponds as a function of radial distance from the center of SPA crater (180 ° E, 50 ° S). The radius of the SPA crater is approximately 40 degree). Locations and estimated area of mare ponds [1] are utilized. The interior of the SPA is divided into several concentric circles with a radial distance of 4 degrees (~ 120 *km/bin*). The total area of mare ponds in a bin is divided by the area of the bin, and then the coverage of the mare deposits are calculated.

FeO and TiO_2 contents of mare ponds:

Methods: In order to clarify the relationship between magma eruption and impact tectonics, the compositional variations of mare deposits are correlated to the impact structure of the SPA basin. Mare regions are selected from the original distribution of Clementine CD-ROM set. Photometric [3] and geometric corrections are applied. The method of Blewett et al. [4] estimating FeO and TiO_2 contents for the hemispherical reflectance data is modified to estimate the contents for the images of bi-directional reflectance. Then, FeO and TiO_2 maps of mare ponds are obtained. In order to avoid the effect of mixing of highland materials and debris from crater wall, the fresh and plain region with the area >10x10 pixels (2 x 2 km^2) are examined.

Results: In Figure 2, FeO and TiO_2 contents of each mare pond are shown as a function of the radial distance from the center of the SPA crater. FeO contents of mare ponds of small areas are dispersed between 11-17 %. In order to avoid the effect of mixing of highland materials, only mare ponds with an area larger than 5,000 km^2 were taken into account. All examined mare deposits in the SPA are classified in Low-Ti basalt type, whereas, in the outside the SPA, TiO_2 content is up to 7.3 % (mare Moscovience), classified into the High-Ti basalt type.

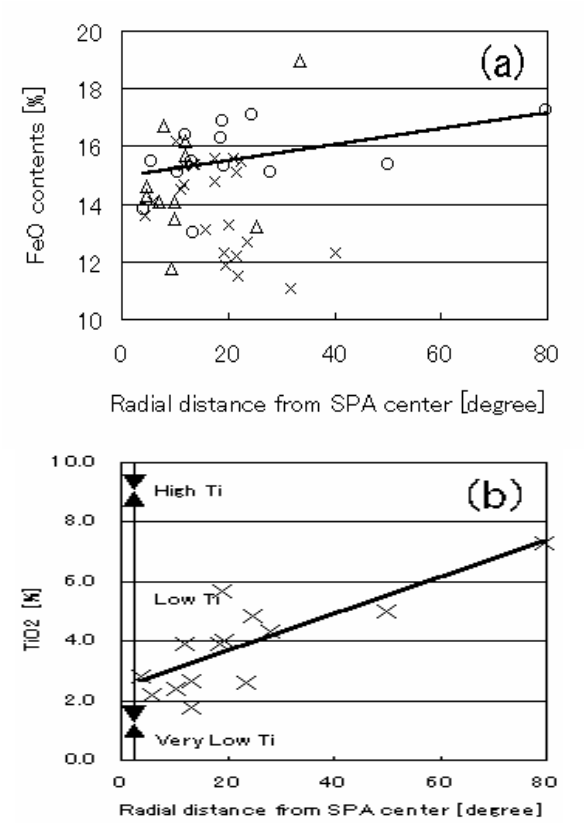

Figure 2. (a) FeO contents of mare deposits as a function of radial distance from the center of SPA crater. FeO contents of mare deposits of areas of > 5,000 km^2, 2,500 – 5,000 km^2, and 0-2,500 km^2 are shown with symbols of ○, △, and ×, respectively. The solid line is a fitting line of 13 mare deposits whose areas are greater than 5,000 km^2. (b) TiO_2 contents of mare deposits as a function of radial distance from the center of SPA crater. TiO_2 contents of mare deposits of areas of > 5,000 km^2 are shown here. Solid line is the fitting line of these data. The radius of the SPA crater is 40 degree.

Discussions:

Petrologic models of the upper mantle indicate that the High-Ti basaltic source is located above the Low-Ti basaltic source [5]. Impact cratering models further indicate that the excavation of the crust materials and possible exposure of the upper mantle [6]. The exposure of the lower crust or the upper mantle is also recognized by high FeO contents of the SPA crater floor [7]. A possible scenario considering these evidences is shown in figure 3. In the SPA center, the upper mantle layer producing the magma source of Hi-Ti basalts may have been heavily brecciated, mixed with crust materials, some ejected, rebounded, and less-pressurized compared to having been in the original depth. Magma chambers could not be developed, and result in a lack of High-Ti basaltic volcanism in the SPA region. On the contrary, outside the SPA, adding to the original setting of the crust and the mantle layers, the SPA ejecta layer overlay. In these regions, magma reservoirs of both High-Ti and Low-Ti basaltic sources could be developed in the upper mantle, and volcanic extrusion from both mantle sources can be possible. They are triggered by the excavation of the large impact cratering, such as, the Moscovience basin, and High-Ti and Low-Ti basaltic volcanism could be observed.

Figure 3. Possible scenario of volcanic activities in/around the SPA region. The model of the upper mantle layers is derived from [5]. The excavation model is from [6]. The boundary of the layers of High-Ti and Low-Ti basalt sources is located in the depth of about 100 *km*. The upper mantle layer of the source of High-Ti basalts may have been highly brecciated and may never have developed magma chambers, in the SPA. Inside the SPA, only Low-Ti basalts are erupted. Outside the SPA basin, both Low-Ti and High-Ti basalt types could be erupted as seen in mare Moscovience.

References:

[1] Yingst R. A. and J. W. Head (1997) *J. Geophys. Res.* 102 10,909-10,931 [2] Greeley, R. *et al*. (1993) *J. Geophys. Res.*, 100 17,183-17,206 [3] Pieters, C. M. et al. (1995) http://www.planetary.brown.edu/clementine/calibration.html [4] Blewett D. P. *et al.* (1997) *J. Geophys. Res.*, 102, 16,319-16,325. [5] Taylor G. J. *et al.* (1991) *Lunar rocks. Lunar Surce Book*, 183-284, Cambridge U. Press, 736pp, Snyder, G. A. *et al.* (1991) *LPSC*, 23, 1,325-1,326. [6]Takata, T.(1996) *LPSC*, 27, 1,307-1,308. [7]Lucey P.G. *et al*. (1998) *J. Geophys. Res.*, 103, 3,701-3,708.

NEW LABORATORY RESULTS ON FIELD SECTIONS AT THE IMPACT CRATER OF ARAGUAINHA (MT, GO, BRAZIL). AREA OF PROXIMAL AND DISTAL IMPACT EJECTA, INCLUDING MICROSPHERULES DATED FROM THE END OF PERMIAN.

J. M. Théry[1], A. Crosta[2], E. Veto Akos[3], E. Bilal[4], K. Gal-Solymos[5] and E. Dransart[6]. [1] 9, Jardin Gabrieli 3700 Tours France – jeanmt15@yahoo.fr - [2]IG, Unicamp 13081-970, Campinas (SP), Brazil – alvaro@ige.unicamp.br [3] E. Veto Akos, II Budapest 1026, ut Baloch Adam 18-6, Hungary - h5980vet@ella.hu [4]Ecole Mines St Etienne – Centre Spin, 158 cour Faurel 42023 St Etienne France ebilal@admunix.emse.fr [5] Eötvös University, Dept. Petrology H-1117 ELTE, 1088 Budapest Churum krt 4/A Hungary. solymos@ludens.elte.hu - EMTT[6] (Etudes Métalurgiques et de Traitement) - 1 avenue du Chater 69340 Francheville France – emttnet@aol.com.

Introduction: The Araguainha Impact crater is located in Brasil in the northeastern part of Parana Basin: latitude -16°77', longitude –52°58'. Its diameter is 40 Km.

W.Engelhardt[1] (1992) and A.P. Crosta[2] (1981) are amist the first with Dietz and French (1972) to reconize, this crater as astrobleme. We have to give a right credit to all geologists, who worked there before.

On the impact crater at Araguainha and neighbouring areas [1], we have obtained new data during our field survey carried out in July 1998 with A. Crosta. The purpose of the present paper is to give an outline of our research. The samples collected within the crater and in neighbouring localities have provided a clear understanding of the stratigraphy of the Permian-Triassic boundary (PTB) at the time of impact.

As a result of a careful choice of twelve new sample locations in the area of the crater itself, we have been able to discern some of the nature and constitutions of the breccia and dikes. Subsequently, the constituents were studied thoroughly by petrographic analyses. The layered nature of the breccia allowed us to establish an order in the deposits. The results from petrographic thin sections and Scanning Electron Microscopy/EDAX studies were compared. We systematically analysed the Landsat MSS and the Landsat Thematic Mapper images (already studied in [2], and [3]), from the outcrop areas, in order to obtain a correct map base for our interpretations.

Results:

The most important results have been obtained from the use of the petrographic diagrams of [4] and [5]. Plots in the Total Alkali Silicates diagram (TAS) are consistent with the QAPF modal classification of granites and of eruptive rock and proposals published before were revised and updated.

In this framework, some of the alkali-rich K granites collected at Araguainha are in reality rhyolites with all their various constituents, rhyo-dacites and andesites. It has become evident that the uplifted K granite of the target rock (basement dated at present 500 to 530 Ma, the red dikes and the breccias ejected and deposited around the area are of the same age. According to field observations on sample locations 6 and 8 (E Veto Akos, written information), the impact related breccias, present in the impact products, are mixed with rhyolitic debris. A volcanic eruption was caused by the impact event at PTB.

We have established the geological build up of the target rocks at the time of the impact event, the severe modification of this build up after the impact and the erosion and weathering phases since the Permian time by studying the signs of shock-waves observed during our field trip and from aerial photographs.

A large, 3 to 4 km in diameter, iron-rich bearing meteorite, fell at Araguainha at the end of the Permian., very close to a mega structure known as the Tranbrasilian Lineament [6] at the boundary between the Guapore Plate (U. Precambrian) and the Goias Plate (Archean to Precambrian). Shearing and thrusting took place at the boundary of an old Cambro-Ordovician granitic trend and the Arnica Mts. The latter were folded during the Guandacol- and subsequent Ocloyica orogenies, the Famatinian cycle, probably at the end of the Ordovician but definitively at the end of Lower Devonian time ([7], [8] and [9]). According to detailed maps of the DNPM of the state of Goias (1986), the Serra Negra Rift in the Araguainha area and at Piranhas near Bom Jardim of Goias was formed along this line of weakness in Western Gondwana. This event took place as early as Lower Llandovery [10]. This tectonic process was initiated by the collision of the Precordillera of Argentina, separated from Laurentia, against the western margin of Western Gondwana [11].

With the ejection of molten granite and rhyolites, a layer of breccia was formed with the largest particles and ejecta near the front of the Arnica Mts. already formed in Devonian times. Those old ranges are at present eroded but retain their former outlines and fold axis. The finer sized ejecta are believed to have been thrown in a southern direction in accordance with the

scheme of [12] and revised by [13], following simulation studies of the growth and movement of particles. As a last stage, we assume a process of volcanism followed by a hydrothermal stage at the northeastern periphery of the crater (sample locations 11 and 12) with a characteristic fluid phase (OHmol, F, CI).

Microspherules Within The Proximal And Distal Ejecta:

The microspherules ejected from the crater are probably included within the smallest ejected particles. We have many examples of this within the Araguainha crater itself and surrounding areas, *e.g*. at Balneario 60 km away from the crater location and in Montividiu, 196 km. towards the southeast. The investigations on proximal ejected particles were carried out at a hill site in the breccia belt identified by the presence of a TV antenna. Here, we have collected some samples (Nb 5) which show the presence of Ni-rich) when analysed by ionic probe IMS (1500 ppm Ni), SEM and elemental spectra. At the same emplacement Hipperttet et Lana (1998 MPS 33, 1303-1309) observed a Rh and Ir enrichment (4x) relative to the indigenous target sediments, where Ir content is only 0.4 ppb.

In Balneario near Alto Garças (MT), just above the thick- stromatolite beds [14], we found nice PDF with 1-2 microns-thick laminae. According to E. Dransart they contain small fluid inclusions, less than 1 micron in size. We have also observed oval quartz, 30 micron in size forming a "ballen", structure. They are "crackled" [15] and provide evidence of an impact origin of the Araguainha crater. They are considered as small ejecta included in the deposits and mixed with gravels and probably pseudotachylites [14]. We have also found diaplectic glass along a dike close to the TV hillside (written information from thin section studies by E. Veto Akos). According to Jean Dejax (Museum d'Histoire Naturelle, Paris) and Rodolfo Dino (Petrobras, Rio, Brazil), a palynological assemblage found in a recent determination, precises the top of Tatarian to Lower Triassic at Montividiu (GO) (written pers.com). We identified, precisely the extraterrestrial microspherules, the shocked quartz and the detailed stratigraphy of the PTB. In addition, these data confirm the age of 247-251 Ma for the distal ejecta in Montividiu (GO), which had been formerly determined by datation of observed fungal event [16].

Summary:

The presence of distal ejecta at the south of the Araguainha impact point at the PTB up to 10-60 Km and even 196 km distant, suggests a large area of distribution of characteristic fallout ejecta.

In addition, according to map data, three to four secondary craters are believed to exist around the main crater in the form of a cluster 25 to 35 km in size. It shows the importance of the Araguainha impact at PTB, already well known as the time of the most important mass extinction of flora and fauna. This worldwide catastrophic event can be emphasized by the impressive belt of extraterrestrial material of the same age around the old Tethys Ocean ([17] and [18]) and if we consider all material containing exraterrestrial microspherules known at Sassayama [19] (Japan), Meishan [20] (South China) and in the Bukk Mountains (hungary)[21], as impact fallout material at the end of Pemian time. We can also add one more recently discovered location in the western Caucasus (pers. com) where we found -Ni/Cr spinels at the Pemian Triassic boundary.

References:

[1] Engelhardt W. et al. (1992) *Meteoritics*, *27*, 442-457. [2] Crosta A. P. et al. (1981) *Rev. Bras. Geosciences*, *11*, 139-146. [3] Crosta A. P.and Thomé Filho (2000) *Post Congr. field trip*, Aft 47, Rio de Janeiro. [4] Mc Donald et al. (1992) *US Geol. Survey Prof. Paper 1523*. [5] Le Bas et al. (1986) *J. of Petro*., *27*, *P3*, 745-754. [6] Brito Neves and Cordani (1991) *Precambr. Res*., *53*, 23-40. [7] Rapela et al. (1992) *in* Gutierrez et al., *Merida, Extramadura*; 21-68. [8] Pankhurst and Rapela (1998) in "The proto Andean Morgin of Gondwana".Geol. Soc. Special Publ. 142; 383p.-London.. [9] Thery JM. (1978) inter. rept. unpublished. S.N.P.A. 120p. Trompette R., 1994 A.A. Balkema Edit. Rotterdam/Brookfield 350p. [10] Gray J. et al. (1982) *Geology*, *13*, *7*, 521-525. [11] Astini R. A. (1996) *XIII Congr. Geol. Argentina*, *III Congr. Expl. Hidrocarburos*, *Actas V*, 509-736. [12] Stoeffler D. (1974) *Forschritte Mineralogie*, *51*, 256-289. [13] Artiemeva (2002) *IX Int. Conf. on Moldavites, Imp. Glass, and Imp. Proc. Frantiskovy-Lazne, Abstract*. [14] Théry et al. (2002) *Ibid.,Frantöskovy-Lazne*. [15] French B. M. (1998) *LPI Contr. 954*, Houston. [16] Visscher et al. (1996) *US Nat. Acad. of Sciences Proceed. 8*, *93*, 2155-2158. [17] Retallack G. et al. (1998) *Geology*, *26*, 11, 979-982. [18] Chateauneuf et Stampfli (1978) *Notes Labo Paleont Univ. Genève, Fasc. 2*, l-l3. [19] Miono et al. (*1973), Nuclear Methods in Physics Research* B75 p 435-439. [20] Jin Y.G. et al. (2000) *Science,* 289, 432-437. [21] G.H. Bachmann et H.W. Kozur ,Conf. 19 int. 2002 *Frantiskovy, abstact.*

TECHNIQUES OF SHOCK WAVE EXPERIMENTS AND DETERMINATION OF HUGONIOT DATA OF SOLIDS. K. Thoma, Fraunhofer-Institut für Kurzzeitdynamik (EMI), Ernst-Mach-Institut, Eckerstrasse 4, 79104 Freiburg, Germany, thoma@ emi.fhg.de

Introduction: In this paper the current techniques used in laboratory shock wave compression of heterogeneous solids [1] will be reviewed with special emphasis on materials used in industrial applications, and on own work at the EMI [2, 3, 4, 5, 6]. These techniques can be fully applied also to geological materials (minerals and rocks).

Laboratory devices for the generation of shock waves: Two major types of techniques are applied for the generation of shock waves at the laboratory scale (e.g. [1]): (1) Air and light gas gun devices and (2) high-explosive devices. The gas gun techniques comprise a wide range of methods ranging from single stage air guns to two-stage light gas guns. The former cover the lowest range of shock pressure to be achieved in solids whereas with light gas guns shock pressure of up to about 100 GPa can be reached depending on the shock impedance of the target material. High explosive set-ups for the generation of plane shock waves can be used in direct contact with the solid target material or preferably in contact with a flyer plate (plane metal plate) which travels a certain distance before impacting the plane surface of the solid to be studied. Both types of techniques can be used for sample recovery devices which operate according to the principle of the momentum trap method in which a metal container prevents the samples from getting desintegrated and dispersed upon impact. The capabilities of the currently used recovery techniques are reviewed.

Measurements of Hugoniot data of solids: Experimentally measured Hugoniot data are of fundamental importance for the quantitative characterization of the shock wave behavior of solids. The relevant experimental techniques focus on the measurement of velocity parameters (impact velocity of the projectile, shock wave velocity and particle velocity in the target). Using the basic Hugoniot equations and specific equations of state the main thermodynamic parameters such as pressure, volume, internal energy and entropy and consequently shock and post-shock temperatures can be calculated from the experimentally determined velocity parameters. The current state of the art and the future directions in this area will be reviewed.

Specific problems of the shock wave behavior of heterogeneous solids: The application of the described basic experimenal techniques and the Hugoniot equation of state data to polyphase solids is not straightforward. The present state of the art is discussed in some detail and with special emphasis on the shock wave behavior of concrete [4, 6] used as a multi-purpose construction material. For this case which appears to be well applicable to geological materials (polycrystalline or polylithic rocks), the combination of shock wave experiments with numerical modeling by computer code calculations [2, 5] will be demonstrated, and it will be shown that this approach leads to significant progress in the understanding of the shock wave propagation in heterogeneous solids.

References. [1] Asay J. R. and Shahinpoor M. (1994) High-pressure shock compression of solids. Springer-Verlag New York. [2] Hiermaier S. and Riedel W. (1997) Numerical simulation of failure in brittle materials using smooth particle hydrodynamics. *International workshop on new models and numerical codes for shock wave processes in condensed media. St Catherine's College, Oxford, UK*. [3] Nahme H., Hohler V. and Stilp A. (1994): Dynamic material properties and terminal ballistic behavior of shock-loaded silicon-nitride ceramics. *Journal de Physique IV, Colloque C8, Supplément au Journal de Physique III, 4,* 237 – 242. [4] Riedel W. (2000): Beton unter dynamischen Lasten. Meso- und makromechanische Modelle und ihre Parameter., Dissertation, Universität der Bundeswehr, München. [5] Sauer M.; Hiermaier S. and Thoma K. (2002), in *Proceedings of the Fifth World Congress on Computational Mechanics (WCCM V)*, July 7-12, 2002, Vienna, Austria, Mang H. A., Rammerstorfer F. G., and Eberhardsteiner J. (eds.) Vienna University of Technology, Austria, ISBN 3-9501554-0-6. [6] Thoma K., Riedel W., and Hiermaier S. (1999) Mesomechanical modeling of concrete shock response experiments and linking to macromechanics by numerical analysis. *European Conference on Computational Mechanics*, Munich.

DIFFERENTIAL STRESS-CONTROLLED DEFORMATION OF QUARTZ DURING AND AFTER HYPERVELOCITY IMPACT - MICROSTRUCTURAL EVIDENCE FROM THE CHARLEVOIX IMPACT STRUCTURE, QUEBÉC, CANADA.

C.A. Trepmann and J.G. Spray , Planetary and Space Science Centre, Department of Geology, University of New Brunswick, 2 Bailey Drive, Fredericton, New Brunswick, E3B 5A3, Canada, trepmann@unb.ca

Introduction The shock wave initiated during hypervelocity impact is essentially a compressive wave with negligible differential stress components [1]. However, this approximation fails at lower shock pressures [1]. Thus, at the distal regions of a crater and during post-shock relaxation, differential stress may play an important role in shock-induced deformation. The deformation mechanisms and the resulting microstructures depend on the temperature and stress condition that rocks are exposed to. Thus, microstructures can provide important information on the conditions, the target rocks experienced during and after hypervelocity impact. Shocked quartz from crystalline target rocks of the Charlevoix impact structure has been studied by optical and cathodoluminescence (CL) microscopy, U-stage and scanning electron microscopy, combined with electron backscattered diffraction (EBSD).

The Devonian Charlevoix impact structure is located about 105 km north of Quebéc city (47°32'N; 70°18'W) along the north shore of the St. Lawrence River. The topographic expression of the ~55 km diameter complex structure, which possesses a prominent central peak, is well defined, although almost all of the crater fill products have been eroded.

Microfabric The shocked quartz crystals reveal *planar fractures* (PFs) (Fig. 1), which are micro-faults along crystallographic planes, e.g., [2]. The shear offset along these gives clear evidence that they are induced by differential stresses.

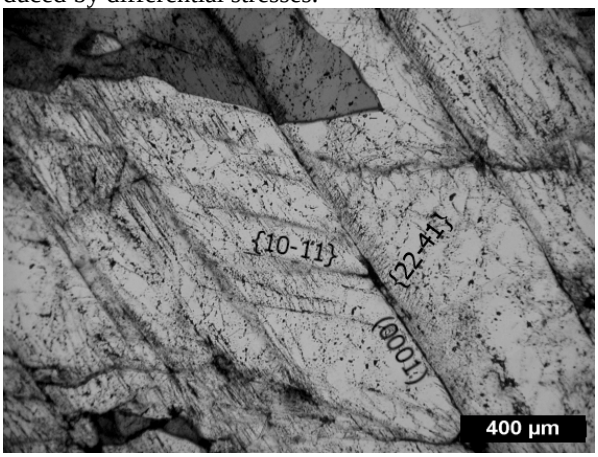

Fig. 1 Photomicrograph (crossed polarised light) of quartz exhibiting PFs with shear offset parallel to (0001).

Planar deformation features (PDFs) parallel to the basal plane dominate at about 8-10 km distance to the central peak. Their frequency decreases with decreasing distance and they are completely absent in rocks of the central peak. The basal PDFs that have been investigated by transmission electron microscopy represent mechanical micro-Brazil twins, e.g., [3]. Additionally, basal PDFs have not yet been unequivocally produced during dynamic high-pressure shock experiments, but at static high differential stress experiments [4]. Thus, it is presumed that they are generated by the differential stress component of the shock wave [5]. The common observation that basal PDFs and PFs only occur at low-moderate shock pressures in distal regions (either in horizontal or vertical distances from the impact point) in a crater indicates that differential stress is in fact a crucial factor in shock-induced deformation in these regions.

A critical resolved shear stress of ~2 GPa on the (0001) plane is required for Brazil twinning [4]. This means that a differential stress of at least 4 GPa is necessary to twin a crystal in a favourable orientation to the maximum stress direction. Even higher differential stresses would be necessary for the twinning of crystals that are not in an optimal orientation to the stress field. Usually, the differential stress in the Earth's crust is expected not to exceed 0.2 GPa. However, during earthquakes it may reach transient values on the order of 1 GPa [6]. Therefore, differential stress conditions during shock in distal regions of an impact crater may be comparable to high stress and strain rate conditions during endogenous-induced deformation, e.g., associated with earthquakes.

The orientation distribution of PFs and PDFs can yield information on the orientation of the stress field. As PFs and basal PDFs are shear stress-controlled, they should optimally occur at an angle of 45° to the highest compressional direction. In contrast, PDFs parallel to rhombohedral planes, $\{10\bar{1}n\}$ with n=1 to 4, which are defined by an amorphous silica phase formed by the transformation of quartz, develop as the result of the high compressional pressure component of the shock wave without the involvement of shear [3]. These rhombohedral PDFs develop parallel to the shock wave propagation direction [2, 3]. However, the stress field is recorded to be highly heterogeneous due to complex interaction of the shock wave with the target rocks and different (de)compressibility of adjacent phases.

Dauphiné twins occur in shocked quartz crystals, visible in orientation contrast images from the SEM (Fig. 2).

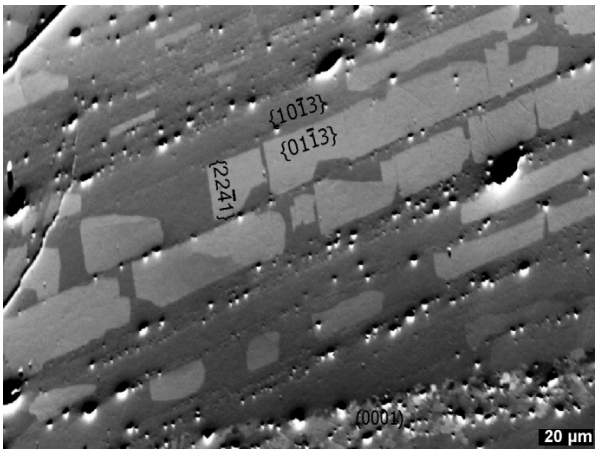

Fig. 2 Orientation contrast image of quartz, exhibiting Dauphiné twin orientation (lighter grey shade).

EBSD measurements reveal the characteristic misorientation angles of 60° and rotation axes parallel to the c-axis. Dauphiné twins are common as shear stress-induced deformation twins in quartz from naturally deformed rocks in a wide range of geological environments, from diagenetic to amphibolite facies conditions. They are also known to be induced during shock experiments [2]. In the Charlevoix target rocks, Dauphiné twins have not been observed in quartz crystals that do not contain PDFs. The twin boundaries are commonly aligned parallel to PDFs (Fig. 2). These observations indicate that the twinning is at least indirectly linked to PDF generation. The twinning might be due to localised shear stress eventually during cooling through the α/β-quartz transition.

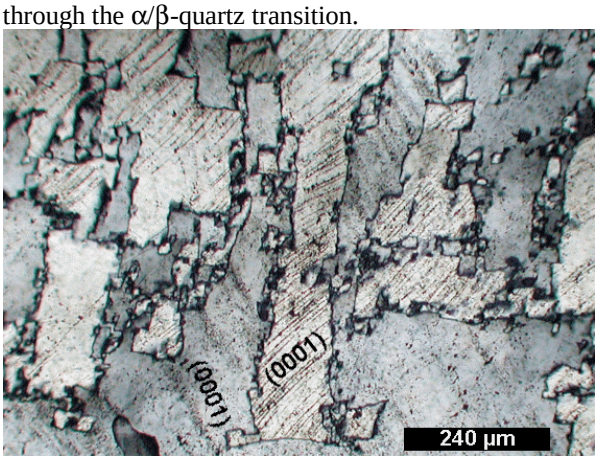

Fig. 3 Photomicrograph (crossed polarised light) of quartz grains with straight parallel grain boundaries in two directions in a high angle to each other.

Conspicuous subgrains, highly sutured grain boundaries and new grains occur in shocked quartz crystals (Fig. 3) The orientation of straight parallel grain boundaries in two directions in a high angle to each other appears to be crystallographically controlled (Fig. 3). These features indicate differential stress-driven glide and climb of dislocations and thus, deformation at temperatures in excess of 300°C and lower strain rates (compared to PDF formation). The fact that some PDFs continue into adjacent - and thus apparently new - grains (Fig. 4), as well as the absence of PDFs in some sutures of grain boundaries, suggests that this deformation took place after the development of PDFs. These findings are reinforced by CL microscopy (Fig. 4): Deformed grains show darker luminescence than the surrounding shocked quartz, which is bluish luminescent. PDFs are visible as a lighter pink colour. Apparently unshocked quartz from the target rocks at large distances from the central peak shows no luminescence. A later thermal event after the impact exceeding 200-250°C is not recorded in the Charlevoix region. Therefore, this crystal-plastic deformation is proposed to represent post-shock relaxation at temperatures still sufficient to allow movement of dislocations.

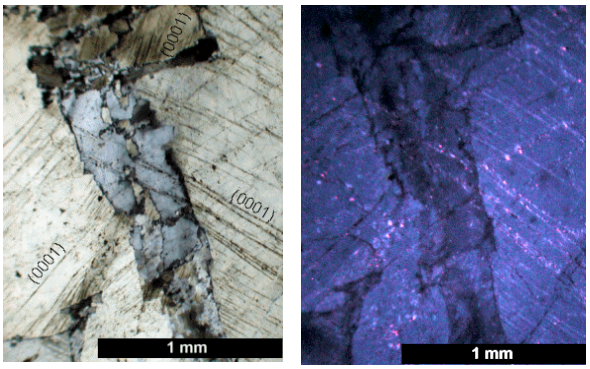

Fig. 4 Optical (left, crossed polarised light) and CL (right) photomicrograph of deformed quartz.

Conclusions The presented quartz microstructures acquired during and after hypervelocity impact are differential stress-controlled rather than induced by the compressional pressure component of the shock wave-associated stress tensor. They provide information on the magnitude of the differential stress and on the stress field during shock. Crystal-plastic deformation is proposed to have been taken place during post-shock relaxation, at temperatures still sufficient and strain rates low enough to allow movement of dislocations. We feel that such observations may be significant for the understanding of the cratering process and shock wave-rock interaction.

References [1] Melosh H. J. (1989) Impact Cratering: A Geological Process. Oxford, New York, 245 pp. [2] Gratz A.J., Nellis W.J., Christie J.M., Brocious W., Swegle J., Cordier P. (1992) Phys. Chem. Minerals 19: 267-288. [3] Goltrant O., Leroux H., Doukhan J.C., Cordier P. (1992) Physics of the Earth and Planetary Interiors 74: 219-240. [4] McLaren A.C., Retchford R.J.A., Griggs D.T., Christie J.M. (1967) Phys. Stat. Sol., 19: 631-644. [5] Leroux H., Reimold W.U., Doukhan (1994) J.-C. Tectonophysics 230: 223-239. [6] Trepmann C.A., Stöckhert B. (2001) Int. Journ.. Earth Sciences, 90: 4-13.

MJØLNIR MARINE CRATER RESULTING FROM OBLIQUE IMPACT: COMPELLING EVIDENCE.
F. Tsikalas[1] and J. I. Faleide[2], Department of Geology, University of Oslo, P.O. Box 1047 Blindern, N-0316 Oslo, Norway, [1]filippos.tsikalas@geologi.uio.no, [2]j.i.faleide@geologi.uio.no

The 40-km-diameter Mjølnir crater is a well-established complex marine impact crater in the central Barents Sea (Fig. 1) [1]. Both geophysical and geological data unequivocally substantiate a meteorite bolide impact at ~142 Ma into an epicontinental basin with 300-500 m paleo-water depth [2, 3].

Obliquity Evidence: It is well documented that the probability for near-vertical and grazing impacts is approximately zero, and that the most probable impact angle of a randomly incident projectile is 45° [4-6]. Following the above estimates, the Mjølnir impact most probably derailed from vertical incidence. In this study, based on the established Mjølnir structure, morphology, and gravity and seismic velocity signatures we search for evidence revealing the impact direction and angle. Such parameters are vital for refining the geographic distribution of ejecta and tsunami-waves, and thus the possible impact-induced regional perturbations and environmental stress.

Elongated crater diameter. The most representative diameter for the near-circular Mjølnir crater was found to be 40 km [7]. We now estimate at 1° intervals the crater diameter around the entire Mjølnir periphery. After normalization to the 40 km average crater diameter, a dominant N-S/NNE-SSW elongation is revealed.

Seismic disturbance asymmetry. For all profiles crossing the center of the structure we have estimated the ratio of the two radii between the crater center and the rim faults (Fig. 2). This provides crater radius asymmetry factors and reveals a consistent asymmetry towards the northward direction (NW/N/NE) in the order of ~1.16, ranging 1.33-1.07. The impact-induced seismic disturbance at Mjølnir has a parabolic bowl-shape at the center of the structure and turns into a shallow broad-brim towards the periphery [8]. The crater radius asymmetry is directly translated to a similar asymmetry in the lateral extent of the shallow broad-brim part of the impact-induced disturbance. This part is not only elongated but also slightly shallower in the same northward-direction (Fig. 2). Furthermore, the parabolic bowl-shaped disturbance at the crater center is related to the transient cavity and reaches, after decompaction, ~5 km in depth. It appears that the transient cavity maximum depth is offset by 2-2.5 km to the south-southwest relative to the geometric crater center (Fig. 3).

Peak-ring character. Although irregular in shape,

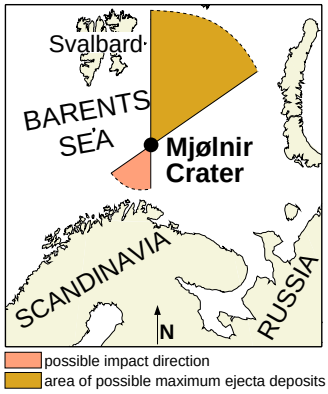

Fig. 1. Mjølnir impact location with possible range of impact direction azimuth and down-range area of maximum ejecta distribution.

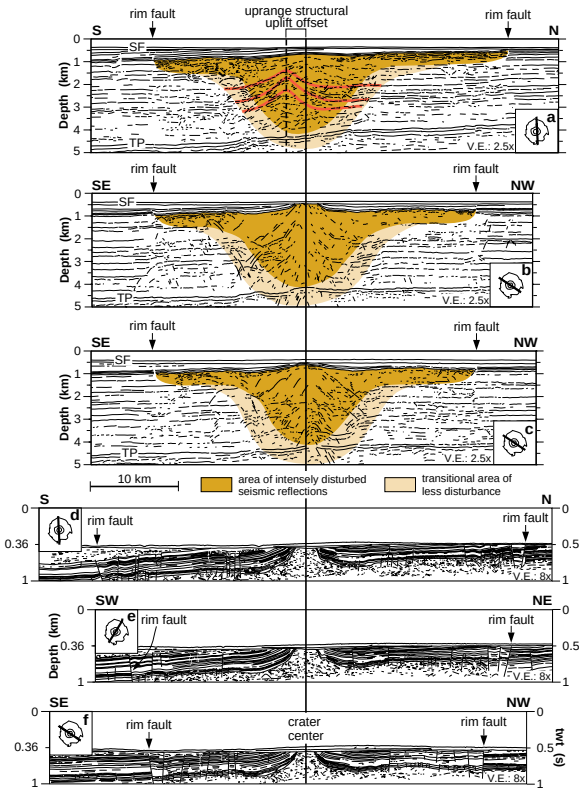

Fig. 2. Interpreted multi-channel (top three) and single-channel (bottom three) seismic reflection profiles stacked along the geometric crater center. In profile (a) selected reflector segments are connected to visualize the clear up-range structural uplift offset. SF, sea floor; TP, Top Permian.

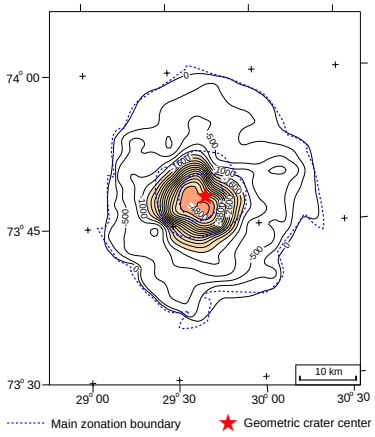

Fig. 3. Morphological characteristics of the decompacted impact-induced intensely disturbed zone, denoting approximately the limit of the annular basin and its maximum depth.

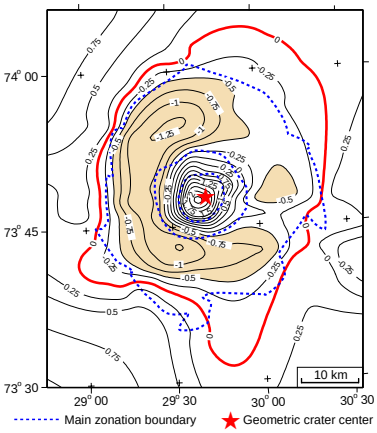

Fig. 4. Residual free-air gravity anomaly map with 0.25 mGal contour interval.

and varying in width from 1 to 3 km, the raised near-arcuate peak-ring relief bounds the outer perimeter of the annular basin and is delineated by opposite dipping faults with 10-20 m throws. This characteristic shape becomes less clear in the N- and NE-directions where the raised relief is breached and the peak ring remains open, being replaced by faults facing the crater center.

Offsets in brecciation and structural uplift. The residual free-air gravity field exhibits a circular anomaly over the structure (Fig. 4): an annular low, with a 45 km outer diameter attaining minimum values of -1.5 mGal over the periphery, and a central 14-km-wide gravity high, with a maximum value of +2.5 mGal [9]. It appears that the 0-mGal gravity anomaly contour exhibits a distinct SW-NE elongated-shape (Fig. 4). In addition, the annular gravity low (<-0.5 mGal, shaded on Fig. 4), which is directly connected with the region of most intense fracturing and brecciation, closely resembles a horse-shoe shape open to the northeast.

It was estimated that Mjølnir experienced ~1.5-2.0 km of structural uplift [8]. We now show that a north-south seismic reflection profile exhibits a 2-2.5 km lateral offset of maximum structural uplift towards the south from the geometric crater center (Fig. 2, profile a). Similarly, the gravity central peak which corresponds to the maximum structural uplift [9] is offset by ~1.5-2 km to the southwest from the geometric crater center (Fig. 4). Furthermore, several seismic profiles reveal a small pull-up of the high-amplitude, originally planar Top Permian reflector beneath the structure (Fig. 2). The mapped traveltime anomaly, 16 km in diameter and +80 ms beneath the central crater [9], is slightly offset by ~2 km to the WSW from the geometric crater center.

Impact Direction and Angle: Our analysis has revealed several evidence that, when combined with the established diagnostic structural and geophysical asymmetries of oblique impacts [e.g, 10, 11], can be related to the impact direction and angle. All evidence for Mjølnir, including the elongated crater diameter, the crater-radius/seismic-disturbance asymmetry, the peak-ring character, and the offsets in brecciation and structural uplift, clearly point to an impact from south-southwest (Fig. 1). A possible impact angle of ~50°, ranging 30°-60°, is found to be representative for the Mjølnir dimensions based on well-established relationships from laboratory experiments and planetary crater studies [5, 12]. Similar values (impact angle of ~45°, range 30°-60°) were obtained using the Mjølnir crater radius/seismic disturbance asymmetry factors in comparison with laboratory results and numerical computations for oblique impacts at various angles [13, 14].

References: [1] Tsikalas F. et al. (1999) *GSA Special Paper, 339*, 193-204. [2] Smelror M. et al. (2001) *Newsletter on Stratigraphy, 38*, 129-140. [3] Tsikalas F. et al. (2002) *Impact Studies (Impacts in Precambrian Shields), Springer Verlag*, 307-321. [4] Shoemaker E. M. (1962) *Physics and astronomy of the Moon, Acad. Press, New York*, 283-351. [5] Schultz P. H. and Gault D. E. (1990) *GSA Special Paper, 247*, 239-261. [6] Shoemaker E. M. et al. (1990) *GSA Special Paper, 247*, 155-170. [7] Tsikalas F. et al. (1998a) *GSA Bull., 110*, 537-552. [8] Tsikalas F. et al. (1998b) *JGR, 103*, 30469-30484. [9] Tsikalas F. et al. (1998c) *Tectonophysics, 289*, 257-280. [10] Schultz P. H. and Anderson R. R. (1996) *GSA Special Paper 302*, 397-417. [11] Schultz P. H. and D'Hondt S. (1996) *Geology, 24*, 963-967. [12] Schultz P. H. (1992) *JGR, 97*, 16183-16248. [13] Gault D. E. and Wedekind J. A. (1978) *LPS IX*, 3843-3875. [14] O'Keefe J. D. and Ahrens T. J. (1985) *LPS XVI*, 629-630.

A new Mid- to Late-Maastrichtian impact in the Raton Basin 100m below the K/T Boundary. P. Turner[1], S. C. Sherlock[2], P. Clarke[3] and C. Cornelius[3], [1]School of Geography, Earth and Environmental Sciences, The University of Birmingham, Edgbaston, Birmingham, B15 2TT p.turner@bham.ac.uk, [2]Department of Earth Sciences, The Open University, Walton Hall, Milton Keynes, MK2 2BY, s.sherlock@open.ac.uk, [3]Evergreen Resources Inc., 1401 17th Street, Suite 1200, Denver, CO 80202, USA.

Introduction: We report a new impact from the Raton Basin, south central Colorado which is 100 m below the well-documented Raton K/T deposit layer in the Berwind Canyon (Figure 1). The Berwind Canyon impact deposit comprises a glass bomb bed, tsunamiite and reworked glass bomb bed. These are found within the Vermejo Formation which is stratigraphically below the Raton Formation that hosts the K/T deposit. Here we present stratigraphic and petrographic details of the Berwind Canyon impact deposit.

Figure 1: A) Regional setting, and B) Chrono- and lithostratigraphy of the Raton Basin.

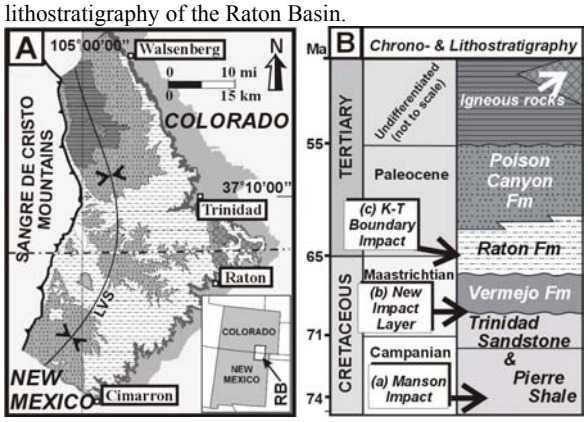

Stratigraphy of the impact horizon: The glass bomb bed, tsunamiite and a reworked bomb bed are overlain by a sequence of shales and intraformational conglomerates with three very competent green massive tuffaceous sandstones interbedded with black shales. The impact deposit comprises irregular glass clasts and bombs with ragged margins, that reach 1m in diameter, and sit within a fluvial sandstone unit. The tsunamiite beds overly the impact deposit, and are buff coloured, poorly sorted sandstones with abundant plant fragments and intraclastic debris flows. These catastrophic layers are associated with at least two wave rippled horizons. These are straight crested with wavelengths up to 25 cm and are considered to have been generated by oscillatory currents associated with the tsunami. Overlying the tsunamiite is a bed of reworked glass bombs. This horizon contains clasts of the glass bombs but these are generally smaller (maximum clast size about 20 cm), are better sorted and more rounded than those in the intial impact deposit. The matrix and succeeding sediments indicate that they have formed by fluvial reworking of the impact deposit (Figure 2).

Figure 2: Reworked impact deposit (glass bomb) within fluvial sandstone.

Impactite: The glass clasts and bombs are black, highly competent and weather to a blocky appearance. The melt contains (in order of abundance) quartz, K-feldspar and rare titanium metal shards, each are angular and with embayed margins, quartz contains a high abundance of fluid inclusions. The glass matrix is reddish brown to black in colour and up to 97% SiO_2 (Table 1).

Table 1: Major element chemical data

	Glass	Glass	Kfs	Metal shard	Metal shard
SiO_2	95.647	96.833	64.523	4.613	6.064
SO_2	0.017	0.008	0	0	0
TiO_2	0.163	0.043	0.001	84.486	87.621
Al_2O_3	01.760	1.950	18.332	1.521	0.343
Cr_2O_3	0.	0	0.026	0.027	0.028
MgO	0.087	0.018	0	0.039	0
CaO	0.106	0.123	0.002	0.178	0.157
MnO	0	0	0.002	0.026	0.011
FeO	0.311	0.062	0.023	6.108	4.277
NiO	0	0.008	0	0.007	0
Na_2O	0.066	0.808	0.361	0.011	0.033
K_2O	0.244	0.101	16.344	0.235	0.028
F	0	0	0	0	0.017
Total	98.406	99.957	99.344	97.251	98.529

Planar deformation features (PDFs) res are frequenct in quartz, as are decorated PDFs, strongly shocked K-feldspar, diaplectic quartz and spherulitic quench tex-

tures formed from quartz/K-feldspar melt, and polycrystalline quartz (Figure 3).

Figure 3: Shock features in Berwind Canyon impact glass: a) PDFs in quartz (U stage image, grain ca. 0.5 mm diameter); b) PDFs in quartz (photomicrograph, grain ca. 0.3 mm diameter); c) quartz/feldspar quench spherule texture (photomicrograph, grain ca. 1mm diameter).

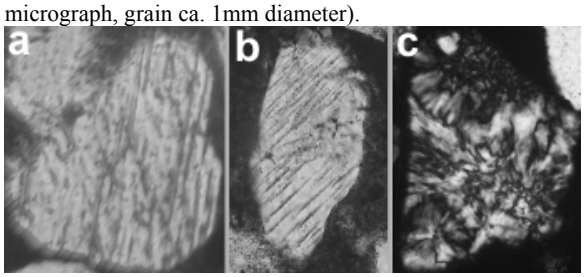

U stage analysis of PDFs conducted by established optical procedures [1] provide rational Miller indices and confirmed their identity as shock effects. Orientation data included high counts of {1121}, {2131} (both 23%) and {1122) (17%) suggesting that the material is 'strongly shocked' [2] with shock pressures estimated to be 30 to 40 GPa due to the occurrence of PDFs and diaplectic glass [3].

Timing of impact: The timing of the Berwind Canyon impact can be constrained to Mid- to Late-Maastrichtian based on the stratigraphy. The impact occurs within the lowest part of the Vermejo Formation near the top of the underlying Trinidad Sandstone The K/T boundary has been identified in Berwind Canyon as a thin tonstein and coal layer within the Raton Formation [4]. This lies ca. 50 m above the newly described Berwind Canyon impact deposit, thus placing it within the Mid- to Late Maastrichtian. The possibility that the Berwind Canyon impact deposit is re-worked Manson ejecta can be discounted since Manson has an age of 73.8 ± 0.3 Ma [5] and distal ejecta are hosted by the Pierre Shale, which is stratigraphically below the Vermejo Formation (Figure 1). In Berwind Canyon, the new impact deposit is separated from the Pierre Shale by the complete thickness of the Trinidad Sandstone, which in this area is 20 m thick. The Berwind Canyon impact clearly occurred between the Manson impact and the K/T boundary. Preliminary $^{40}Ar/^{39}Ar$ data from shocked K-feldspars within the glass indicate an age of 68 Ma or younger. Current and ongoing $^{40}Ar/^{39}Ar$ work will provide an accurate and high-precision age for the Berwind Canyon impactite horizon.

Implications: The Berwind Canyon impact deposit is significant in that it occurred prior to Chixculub in the Late Maastrichtian and is thus another reported impact, in addition to Boltysh in the Ukraine [6], occurring at or near to the end-Cretaceous. This may have implications of the end-Cretaceous mass extinction, depending on the precise age it may be necessary to re-examine the long-held belief that Chixculub alone caused sufficient environmental perturbation and sudden catastrophic extinction [e.g. 7].

References:

[1] Engelhardt W. and Bertsch W. (1969) *Contribs. Min. Pet., 20*, 203-234. [2] Stöffler D. and Langenhorst F. (1994) *Meteoritics and Planet. Sci., 29,* 155-181. [3] Stöffler D. (1971) *JGR, 76,* 5541-5551. [4] Pillmore C.L. and Flores R.M. (1987) Geological Society of America Special Paper, 209. [5] Izett G.A., Cobban W.A., Obradovitch J.D. and Kunk M.J. (1993) *Science, 262*, 729-732. [6] Kelley S.P. and Gurov E. (2002) *Meteoritics and Planet. Sci., 37*, 1031-1043. [7] Smit J. (1999) *Ann. Rev. Earth and Planet. Sci., 27,* 75-113.

NUMERICAL MODELLING AND PETROPHYSICAL CONSTRAINTS ON THE MAGNETIC SIGNATURE OF IMPACT STRUCTURES. H. A. Ugalde[1], N. Artemieva[2], B. Milkereit[3], [1]Department of Physics, University of Toronto, 60 St. George Street, Toronto, ON M5S 1A7, Canada, ugalde@physics.utoronto.ca, [2]Institute for Dynamics of Geospheres, Leninsky pr., 38, bldg. 6, 119334, Moscow, Russia, nata_art@mta-net.ru, [3]Department of Physics, University of Toronto, 60 St. George Street, Toronto, ON M5S 1A7, Canada, bm@physics.utoronto.ca

Introduction: The magnetic anomalies over impact structures are analized, and constrained by paleomagnetic data and numerical modelling. The processes that lead to magnetic anomalies on impact structures are addressed.

Magnetization on Impact Structures: [1,2] propose that impact structures are characterized by a magnetic low due to a reduction in magnetic susceptibility However, analysis of magnetic anomalies over many impact structures shows that a common attribute is a disruption of main magnetic trends, high amplitudes and short wavelengths.

Large Impact Structures like Sudbury (1.85 Ga age, 250 km diameter), Vredefort (2,006 Ma age, 300 (?) km diameter), Chicxulub (65 Ma age, 180-300 km diameter)and Manicouagan (214 Ma age, diameter ~ 100 km), and mid-size ones like Ries (15 Ma age, 24 km diameter), Lake Bosumtwi (1 Ma age, 10 km diameter), all exhibit this high frequency and high amplitude pattern on their magnetic signature.

Magnetic Related Processes: The magnetic signature observed on large impact structures can be the aggregate of three effects: (1) A secondary remnant magnetization (shock remnant magnetization, SRM) induced by the high pressures of the impact (>30 GPa), if there is enough occurrence of natural remnant magnetization (NRM) carriers on target rocks (e.g. Manicouagan [3], Slate Islands [4]); (2) recristallization of non-magnetic rocks towards more magnetic facies (therefore melt will have a higher magnetic susceptibility than the pre-impact target rocks), increasing magnetic susceptibility (e.g. Chicxulub). This will be controlled by the oxygen fugacity and the cooling speed on first order, and only secondary by bulk chemistry [5]; rapid cooling allows most of the volatiles to escape and Fe, Ti oxides stay in solid solution in equilibrium, facilitating low magnetic susceptibilities; on the other hand, high magnetic susceptibilities can be reached with the same chemical composition, but with a slower cooling rate. Biotite and amphibole can decompose to an assemblage of phases that often contain magnetite, when they are exposed to high postimpact temperatures [6], which will also produce high magnetizations; and (3) hydrothermal alteration processes favoured by impact-induced brecciation, the impact and/or the melt layer as a heat source and the presence of fluids. This lead to the acquisition of a chemical remnant magnetization (CRM) in the direction of the ambient field [1]. Fracturing of the target rocks permits the circulation of hydrothermal fluids, and the presence of oxygen favours higher magnetization intensities [5].

Chicxulub. On the Chicxulub impact crater, a meteorite hit a non-magnetic carbonate platform, but still large magnetic anomalies can be seen. Remnant magnetization intensities are small (10^{-4}A/m, [7] and magnetic susceptibilities can be as large as $1200x10^{-5}$ S.I. towards the base of the suevite packages, suggesting alteration due to a hydrothermal system [7]. The melt layer shows magnetic susceptibilities one order of magnitude smaller than that, which can be interpreted due to the non-magnetic nature of the pre-impact rocks. Boreholes drilled by the Universidad Nacional Autonoma (UNAM) were unable to confirm any indication of SRM, though they were located on the borders of the structure, where SRM should not have been acquired.

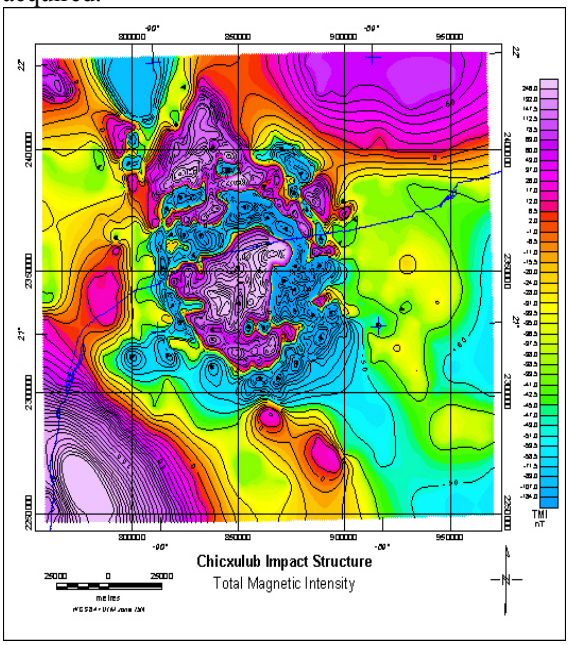

Fig. 1: Total Magnetic Intensity over Chicxulub Impact Structure.

Lake Bosumtwi. Although regional features partially mask the more circular magnetic signatures of the Bosumtwi impact structure, high amplitude and

high frequency anomalies appear on the NE and SW of it. [8] measured susceptibilities ~$3.3x10^{-5}$ SI and NRM of 36.8 mA/m on suevites. Target rocks showed susceptibilities of $2.3x10^{-5}$ SI and NRM of 0.14 mA/m. [8] suggest that the Bosumtwi structure, with its Fe rich target (0.5-9.2 wt% of Fe_2O_3), could yield melt rocks with high magnetization. High magnetizations are observed on the northern part of the lake. [8] links the presence of a biotite-rich granite intrusion on that part of the lake with ferromagnetic iron oxides decomposed from biotite by the shock; then the suevites on that part of the structure may have acquired their NRM by postshock thermochemical processes.

Lake Wanapitei: this structure was published as a ~7.5 km diameter impact structure by [9]. However, new geophysical data shows that if it was originated by an impact, its diameter can not be larger than 3 km [10]. Since no paleomagnetic and/or borehole investigations have been done on it, there is no direct evidence supporting the reason for the disruption of the main magnetic trends on the centre of the structure. Numerical modelling limits the occurrence of melt and recristallization to r<500m from the centre of the structure, then the main mechanism for the observed magnetic signature might be hydrothermal alteration.

Numerical Modelling: Another approach to uncover the source of the magnetic anomalies is the use of Numerical Modelling. Maximum pressure and temperature estimations can be linked with geological and physical/chemical processes that lead to different geophysical signatures. Then, the source for the observed magnetic anomalies can be divided into different units and/or processes: melt, breccia, and post-impact alteration. Numerical modeling for intermediate-size structures (4<D<20 km) is performed (1) with the SALE code [11,12] to receive final crater shape after a vertical impact, and (2) with the SOVA code [13] to model an oblique impact. ANEOS [14] equation of state for granite [15] is used to describe both the target and the projectile. For a 10 km final-diameter structure, pressures larger than 30 GPa (SRM) are approximately restricted to r<1 km and depths<1.7 km. Pressures higher than 50 GPa (rock melting) are confined to r<0.5 km and depths<1.2 km. Therefore, SRM and melt are confined to small areas, sometimes not even discernible by a regional airborne magnetic survey, and easily removed by erosive processes. Hydrothermal alteration induced by fluids circulation on the brecciated and fractured rocks can still increase or reduce magnetic susceptibilities due to recristallization, and lead to the acquisition of a CRM. No matter the type of sediments that fill the crater, their magnetic susceptibilities will be smaller than on the pre-impact target rocks and the main feature will be a disruption of main pre-impact magnetic trends (e.g. Deep Bay [1] and Wanapitei Lake in Canada [10]).

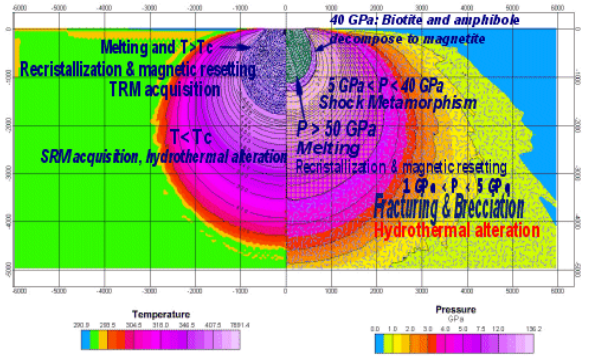

Fig. 2: Maximum pressure (right) and temperature (left) estimations from numerical modeling results [9], with magnetic processes involved. Particles at their initial position.

Conclusion: the magnetic signature over impact structures is characterized by high frequencies and high intensities. The main factors that will define the shape of the anomaly are: (1) *Size of the structure:* defines the amount of melt and the extent of the recristallization and magnetic resetting area; (2) *Hydrothermal alteration:* triggered by brecciation and the presence of water, depending on the oxygen fugacity and cooling rate, it will increase or reduce the magnetization of rocks; (3) *Presence of a secondary Shock Remnant Magnetization (SRM):* it is confined to the centre of the structure, and depending on its intensity and the magnetic latitude, it can greatly modify the location of the positive & negative components of the magnetic dipoles.

References: [1] Pilkington & Grieve, *Reviews of Geophysics*, 30, 2, p.161-181, 1992; [2] Scott, R. et. al., *Meteoritics & Planetary Science*, 32, 293-308, 1997; [3] Coles, R.L., J. F. Clark, *JGR*, v. 83, no. B6, p. 2805-2808, 1978; [4] Halls, H.C, *Geophys. Jour. of the Royal Astr. Soc.*, 59, p. 553-591, 1979; [5] Grant, F.S., *Geoexploration* 23, p. 303-333, 1984; [6] Chao, E.C.T., in *Shock Metamorphism of Natural Materials*, 1968; [7] Rebolledo, M. Unpublished Ph.D. Thesis, UNAM-Mexico, 2001; [8] Plado, J. et. al., *Meteoritics & Planetary Science*, 35, 723-732, 2000; [9] Dence, M.R. and Popelar, J., *Geol. Assoc. Can., Sp. Pap. 10,* p.117-124, 1972; [10] L'Heureux et. al., *CGU Expanded Abstracts.*, 2003; [11] Amsden, A.A. et. al., *LA-8095 Report*, 101p., 1980; [12] Ivanov, B. et. al., *International Journal of Impact Engineering*, v.20, 411-430, 1997; [13] SHuvalov, V.V., *Shock Waves* 9, p. 381-390, 1999; [14] Thompson, S.L. and Lauson, H.S., *Report SC-RR_71 0714*, 119p., 1972; [15] Pierazzo et. al., *Icarus*, v.127, 498-523, 1997.

IMPACT INDUCED HYDROTHERMAL SYSTEM AT KÄRDLA CRATER: DEVELOPMENT AND BIOLOGICAL CONSEQUENCES. E. Versh[1], K. Kirsimäe[2], A. Jõeleht[3], J. Plado[4]; [1,2,3,4] Institute of Geology, University of Tartu, Vanemuise 46, Tartu 51014, Estonia ([1]desty@ut.ee, [2]arps@ut.ee, [3]ajoeleht@ut.ee, [4]jplado@ut.ee)

Introduction: Kinetic energy released to the target by a meteorite impact results in the heating-to-melting and vaporization of the projectile and target rocks which then starts to cool to the ambient conditions. In dry environments the heat loss occurs mainly by conduction and radiation transfer. If the water is present at the crater site the cooling can also include convective heat transfer by a hydrothermal circulation system. Evidences of such system have been found at many terrestrial craters [1] and it is suggested for extraterrestrial craters as well [2].

Impact induced hydrothermal systems are important to study in many aspects. First, cooling and development of such systems is still at debate. In most described cases these systems form in and around the craters central uplift (e.g. Kärdla, Puzhes-Katunki, Siljan) whereas in others they are recognized only at the crater rims (e.g. Haughton). Secondly, mineral deposits formed and/or modified by these hydrothermal fluids represent significant economical interest (e.g. Sudbury). Thirdly, in recent years profound studies have been made on thermal side of the impacts, as they may create new environments for life to evolve [3], which is of great interest in respect to search for possible extraterrestrial life.

In this contribution we report a complex geological observation, modeling and biological study about post-impact cooling of a medium-to-small scale Kärdla impact crater in Hiiumaa Island, Estonia. The Kärdla crater is 4 km in diameter and ~540 m deep with a central uplift exceeding 150 m height above the crater floor. It formed in a shallow (<100 m deep) epicontinental Ordovician sea ~455 Ma ago into a target composed of thin siliciclastic and carbonate sediments covering crystalline basement [4].

Mineralogy: Kärdla crater is an example of an impact induced hydrothermal system developed in the fractured basement rocks at the central peak and in surrounding breccias. The hydrothermal water-rock interaction in heated impactites is characterized by a complex of clay – K-feldspar – silicate - carbonate mineralization assemblage. The most intensive alteration is found in breccias and shattered basement immediately at the central uplift. Mineralogical and fluid inclusion data suggest post-impact temperatures in heated breccias varied from peak ~440°C to ambient conditions [5] (Fig. 1).

The parasequence of the hydrothermal mineralization represents a sequence of minerals formed in a single event of the gradually decreasing post-impact temperature. Mineral associations suggest at least three evolutionary stages: (1) early vapor dominated stage (>300 ºC), which resulted in the precipitation of cryptocrystalline adularia type K-feldspar and quartz; (2) main stage (300 to 150(100) ºC), with development of two-phase (vapor to liquid) zone with chlorite/corrensite, submicroscopic idiomorphic (blocky) K-feldspar and quartz formation; and (3) late liquid dominated stage (<100 ºC), with calcite I, dolomite, quartz, calcite II, chalcopyrite/pyrite, Fe-oxyhydrate and calcite III precipitation.

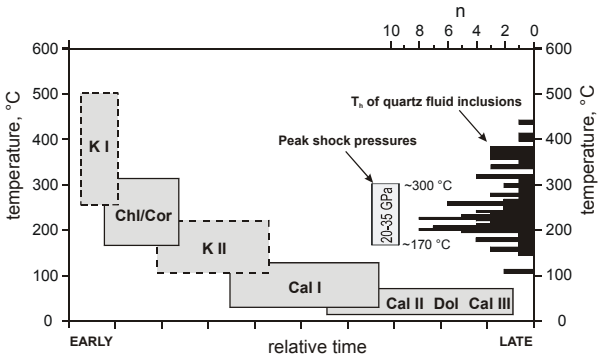

Fig 1. Post-impact hydrothermal mineralization parasequence and post-impact temperatures in Kärdla crater. Shock pressures (20-35 GPa) from [6] and histogram of aqueous (H2O-NaCl) quartz fluid-inclusion homogenization temperatures (T_h) from [5] are shown at the RH side. K - K-feldspar, Chl/Cor - chlorite/corrensite, Cal - calcite, Dol - dolomite; I, II, III - 1st, 2nd and 3rd generation. Formation temperatures for chlorite-corrensite and carbonate minerals are estimated form geothermometry and stable isotope composition, respectively.

Impact and geothermal modeling: The SALE hydrocode was used to simulate formation, modification and the impact heating in Kärdla crater. Modeling was done using ANEOS equation of state algorithm. Modeling results are in good agreement with mineralogical and fluid inclusion observations and suggest maximum post-impact temperatures of 400-600°C.

The results of transient fluid flow and heat transfer simulations in Kärdla suggest that immediately after the impact the temperatures in the hydrothermally most altered central area were well above the boiling point (200-250°C depending on hydrostatic pressure at location). Due to efficient heat loss at groundwater vaporization front the vapor-dominated area disappears in a few tens to hundreds of years. The overall cooling to ambient temperatures in the deeper parts of the central uplift may have lasted for thousands of years. In crater depression and rim areas the initial temperatures, suggested by impact modeling, were much lower – from 150°C to ambient temperatures. However, the mineralogical data suggest that the temperatures at the rim have been locally higher (up to 200-300°C) in fracture zones and suevite pockets. These higher temperatures could have lasted for few years after the impact only. In the early stage, convective heat transfer prevails whereas at the later stage conduction dominates. This is due to the convection/conduction ratio, which depends on a rock permeability structure, and because the permeability of shattered rocks in an impact crater decrease in time due to the closure of pores by hydrothermal mineralization. It is relevant that different parts of the crater cool at different rate, e.g. in comparable depth the rocks in central uplift are not cooling as fast as rocks near the ring depression, and precipitation of the same hydrothermal mineral varies in time and space.

Prospects for life: Geothermal models suggest that in the central uplift area conditions for thermophilic microorganisms (temperatures <100°C) were reached already in less than 500-1000 years after the impact (Fig. 2). Suitable conditions for hydrothermal microbial communities were established shortly (tens to few hundreds of years as maximum) after the impact in the most part of the crater. In the central uplift area the microbial colonization was inhibited for about a thousand year. However, this was the area, which retains the optimum temperatures (60-80°C) for thermophiles for the longest period.

So far, we have not found any direct evidences of microbial colonization in hydrothermal fracture systems at Kärdla.

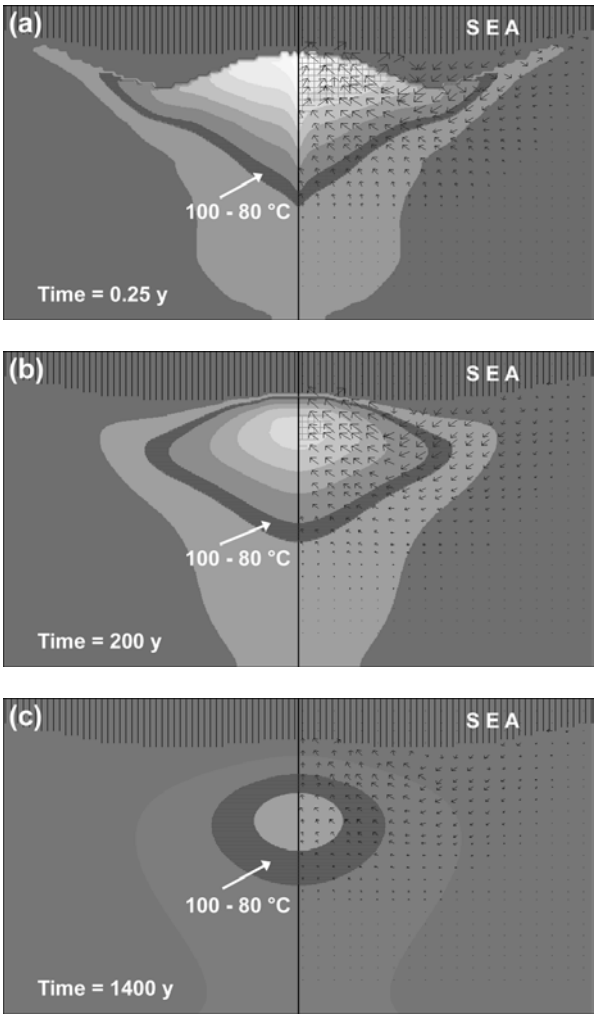

Fig. 2. Temperature field evolution in Kärdla crater rocks: (a) 0.25 years, (b) 200 years and (c) 1400 years after the impact. Isoterms are drawn after every 50 °C, from 400 °C down to 50 °C. Temperature field between 100 and 80 °C (as most suitable for hyperthermophiles) is marked with darker color.

References: [1] Naumov M.V. (2002) *Impacts in Precambrian Shields*, pp. 117-171. [2] Newsom H.E. (1980) *Icarus 44*, 207-216; [3] Cockell C.S. and Lee P. (2002) *Biol. Rev.* 77, 279-310 [4] Puura V. and Suuroja K. (1992) *Tectonophysics*, 216, pp. 143-156. [5] Kirsimäe K. et al. (2002) *MAPS*, 37, 449-457. [6] Puura et al. (submitted) *MAPS.*

THE FEATURES OF THE POPIGAI: A GUIDING KEY FOR LARGE-SCALE IMPACT CRATERING PHENOMENA. S. A. Vishnevsky, Institute of Mineralogy and Petrology, Novosibirsk-90, 630090, Russia <nadezhda@uiggm.nsc.ru>.

Introduction: The simple model of cratering is well established, and typical features of the simple craters (shape, rim, overturned flap, ejecta deposits, etc.) are studied in details. However, the theory of impact cratering cannot explain some features of large complex craters [1,2]. For example, in spite of the numerous investigations, an origin of ring and central uplifts is still a matter of debates [2,3]. Some other features of the craters are less debatable but not less important; their origin is also an open question. One of the ways to have a progress here might be based upon the field investigations and attempts to explain the debatable features. In this connection, some geological observations on the Popigai astrobleme (PA) and their interpretations may be of definite interest. Following to its size (100 km), young age (~35 Ma), well preservation and good exposure, as well as to plenty of impact formations and diversity of target lithologies, the PA is a unique test site for the theory of large-scale cratering. Some key geologic features of the PA are presented below. Their description is based upon our nomenclature of the PA impact formations [4,5].

Description:

1. Impact diatremes and horsts are specific impact-induced tectonic structures, known in the PA only [5 and ref. therein]. They are locally present in Cambrian terrain in the west, northwest, east and southeast surroundings of the crater, 3 to 5 km far from its tectonic rim. Impact diatremes are pipe-like bodies up to 3.5 km in diameter, filled up with a chaotic mixture of fragments (from the pebble size up to the blocks of 700 m across) derived from various target lithologies. Impact horsts, from 300 m to 2 km in size, are made up of Proterozoic arenites. The elongation of both the structures, if present, follows to regional W-NW faulting trend. Except for the "gries" breccia, no other traces of shock metamorphism (SM) are recognized in these structures.

2. Proximal ejecta deposits are very poor in close vicinity around the PA, except for the north surrounding of the crater where they have a wide enough extent and are observed to up to 20 km from the tectonic rim of the crater. At the same time, the relics of pre-impact Paleogene planation surface and old river valleys with remnants of loose Mesozoic sediments are preserved around the crater. So, the lack of the proximal ejecta blanket cannot be explained by erosion only and indicates any specific feature of the origin of the PA. At this, there is an evidence of more distant, up to 500 km far from the crater, ejecta deposits, traced by the strewn field of impact diamonds [6]. Besides it, a global dissemination of the PA distal ejecta deposits is well grounded [7], and at least one of the Eocene/Oligocene impactoclastic horizons can be related to the Popigai impact event.

3. The principle of "reversal stratigraphy" is not valid for the explosion cloud deposits (suevite formations) in inner part of the crater. Clastic material derived from the loose Mesozoic target lithologies dominates in the deposits. Suevite megabreccia formation is especially paradoxical in this respect. It forms a belt in the middle part of the crater and contains a number of large, up to 80 m in size, lumps of loose, mainly Cretaceous, Mesozoic target lithologies. Suevite megabreccia is known in the PA only [5,8].

4. Two principally different spatial sources of the material are another paradoxical feature of the major part of the PA suevites, and of the suevite megabreccia in the first turn. These source materials are: 1) weakly- or non-shocked at all clasts of mainly loose sedimentary target lithologies derived from the middle and marginal zones of the growing crater (traces of shock metamorphism either are absent at all, or are limited by "gries" breccia and shatter cones only); 2) strongly-shocked (up to the state of high-temperature impact melt) material of Archean gneisses, derived from the inner part of the growing crater [5,8]. A model of simple mixing in the ejecta plume cannot be applied for the origin of large (not less than 500-700 km^3 in volume) body of the suevite formations of the PA, accompanied by a lack of the "reversal stratigraphy".

5. *Evidences of the dynamic interaction* between the components *in a dense/condensed state of the matrix* are once more paradoxical features of the suevite megabreccia formation. This interaction took place while the matrix of the megabreccia was already lithoid-and-plastic, and even lithificated [5,8]. Traces of fast forced movement of the target rock lumps in this matrix are among the evidences. Streamlining deformations and dragging trains behind the lumps indicate this movement. Evidences of turbulent mixing between various kinds of suevites, which compose the matrix of the formation, are also very common. "Breccia-within-breccia" relations when fragments of one suevite are cemented by another suevite are also observed in the megabreccia matrix. Proponents of volcano-tectonic origin of the PA used this feature as an evidence of its prolonged multiphase origin [9].

6. Sharp contacts between various suevites are observed by places within the suevite strata of the PA. At

first glance, this feature is also consistent with the volcano-tectonic origin of the structure.

7. *Bedding of the suevites on the Archean gneisses* is often observed on the crest of the inner ring. Moreover, mixtures of gneiss lumps and suevites are known in some places here. It shows that the ring originated very quickly, while a part of the explosion cloud material was still either in flight, or in a mobile state during the collapse and emplacement.

Interpretation: Simple models of cratering cannot explain the features of the PA geology described above (items 1 to 6). Our interpretation is made on the basis of the hypothesis of the dynamic barrier (HDB); we suppose that this barrier was originated in the explosion cloud of the Popigai impact event [5,8]. Following to HDB, the subsurface lag of the shock wave front in soft surficial Mesozoic target rocks originated in middle and marginal zones of the growing crater. Propagation of attenuating shock wave in this zone was accompanied by the elastic precursor. This lag originated as a result of a density contrast between the Mesozoic (~1.8-2 g/cm^3) and other target lithologies (~2.6-2.8 g/cm^3). With application of simple cratering mechanics after [10], we can conclude that due to the lag, the soft Mesozoic lithologies were ejected along high-angle to vertical trajectories; as a result, a torus-shaped cloud of low-shocked rock fragments rose vertically up above the middle and marginal zones of the growing crater. This cloud would function as a dynamic barrier for expanding conical plume of high-speed strongly shocked ejecta derived from Archean gneisses in inner part of the crater.

A scarcity of proximal ejecta deposits around the tectonic rim of the PA can be explained by means of HDB (a screen effect of the dynamic barrier). The same screen effect of the barrier would serve also as a course for the local sharp contacts between various suevites. An origin of the suevite megabreccia in the middle zone of the crater, a lack of the "reversal stratigraphy", and two principally different spatial sources of the material for the suevitic formations can be explained by means of HDB also (colliding at the dynamic barrier and intensive mixing between the high-speed and strongly-shocked crystalline rock ejecta and the torus-shaped cloud of Mesozoic fragments). Evidences of the dynamic interaction between the lumps and matrix of the suevite megabreccia, as well as the traces of turbulent mixing between various kinds of suevites and "breccia-within-breccia" relations between them in the matrix of the megabreccia can be explained by the colliding of ejecta at the dynamic barrier also (a partial condensing/compacting of the suevitic material to a dense lithoid and even lithified state, and a dynamic interaction between them). More detail interpretation of the PA geological features on the background of HDB is discussed in [5,8].

Origin of impact diatremes and horsts can meet an explanation by means of subvertical ejection also: these specific impact-induced tectonic structures are the evidence for subvertical shock impulses transmitted from the deep interior of the growing crater.

Very fast origin of the inner ring of the Archean gneisses is considered as a result of coherent centrifugal plastic flow of the basement rocks under the crater bottom. It took place at the excavation stage. Its origin is similar to the origin of the base stage of the rim in simple craters. Following to this interpretation, the inner ring of the PA is just a rim of the inner crater, elaborated in the crystalline basement rocks. Other models of its origin (isostatic relaxation, gravity collapse, etc.) seem invalid according to the very fast rising up of the ring.

Of course, some our interpretations presented above would not be possibly confirmed later. Anyway, the discussion on the subject will be useful for the better understanding of large-scale impact cratering

References: [1] Spudis P. D. (1993) The geology of multi-ring basins. N.Y., Cambridge University Press, 263 p.; [2] French B. M. (1998) Traces of catastrophe. LPI Contribution #954, 120 p.; [3] Melosh H. J. (1989) Impact cratering: a geologic process. N.Y., Oxford University Press, 245 p.; [4] Vishnevsky S. A. (1981) In: Impactites (Moscow University Press), p. 171-184 (in Russian); [5] Vishnevsky S. and Montanari A. (1999) GSA Special Paper #339, p. 19-59; [6] Vishnevsky S. A., et al. (1987) Impact diamonds: their features, origin and significance. Novosibirsk, Academy Press, 110 p. (in Russian & English); [7] Montanari A. and Koeberl C. (2000) Impact Stratigraphy. LNES, vol. 93, Berlin, Springer-Verlag, 364 p.; [8] Vishnevsky S. A. (1994) Suevite Megabreccia - a new type of the Popigai explosion cloud deposits. Novosibirsk, Academy Press, 66 p.; [9] Polyakov M. M. and Trukhalev A. I. (1974) Izvestiya Akademii Nauk SSSR, Geology, 4, p. 85-94 (in Russian); [10] Gault D. E., et al. (1968) In: Shock Metamorphism of Natural Materials, Baltimore, Mono Book Corp., p. 87-99.

SUEVITE-TAGAMITE MEGAMIXTURES: AN IMPACT FORMATION ON THE FLOOR OF THE POPIGAI SUEVITE STRATA. S. A. Vishnevsky, Institute of Mineralogy and Petrology, Novosibirsk-90, 630090, Russia <nadezhda@uiggm.nsc.ru>.

The Popigai suevites and the underlying impact formations: The Popigai explosion cloud deposits (the suevite strata) are well preserved in inner basin and annular trough of the crater and include several types of suevite formations. The Parchanai suevite formation, or PSF (the volume and nomenclature of Popigai impact formations is based upon our classification [1]), occupies the lower part of the strata and contains a number (up to 50-70 % of the rock volume) of glass particles, mainly of lapilli-size. The rest of the rock is a matrix made up of mainly psammitic fragments of target lithologies, among which the clasts of the soft Mesozoic rocks dominate. Parchanai suevites came from the lower part of the explosion cloud and were the first to be deposited in a relatively hot state; they are well lithified and strongly altered. In the field, the PSF rocks are well distinguishable from any other suevites due to pumice strongly altered light-greenish-yellow glass fragments. Syngenetic (i.e., originated during cratering) relations of the PSF with underlying bottom impact formations are the next: 1) in some places of the inner ring of the Archean gneisses the suevites either were emplaced directly on them, or served as a cementing matrix of the gneiss fragments; 2) in some other places of the ring and the crater margin the suevites are emplaced on the impact melt rocks – tagamites, or are included as small irregular bodies in the uppermost part of the tagamite sheet and megabreccia. Epigenetic (i.e., originated during post-impact modification of the crater) relations of the PSF with the bottom impact formations are the next: 1) the suevites are the wall rocks for numerous intrusions of the buried tagamite melt; 2) sheet-like and cover tagamite bodies in and on the suevites are known on the slopes of the inner ring and in some places of the crater; they originated as a result of gravity slumping and melt flow from the highlands.

Megamixtures of the Parchanai suevites and tagamites: Specific syngenetic relations between the PSF rocks and tagamites are known in some places of the west and south-east sectors of the inner ring and adjacent areas, especially in the riverheads of Balagannakh-R., Namsik-Daldyn-R. and Balagan-Yurege-R. There is a kind of transition zone between the suevites and underlying tagamites represented by a chaotic mixture of irregular and swirled tagamite and suevite bodies up to several tens of meters in size. The type of the contacts (a complex interfingering and stream-vortical relations) indicates the turbulent interaction between the contacting masses at still mobile and plastic state.

Small, up to 2 meters in size, tagamite bodies are rarely known in the PSF at various places of the crater. However, the impactites described above and defined here as the suevite-tagamite megamixtires occupy extensive enough (of many square kilometers) areas and can be distinguished as a special allogenic impact formation. In a mode of transportation and deposition of the material this formation is intermediate between the suevites themselves and the bottom centrifugal flows of the tagamite melt.

As we suppose, the partial disintegration of the tagamite melt into large lumps at the stage of its centrifugal displacement is a result of any regular process, but not a result of any random fluctuations in moving near-bottom flow. The explosive disintegration of the impact melt at the excavation was already analyzed [2], and these authors come to the conclusion on the important role of the volatiles in this process. In particular, they found an importance of free porous water derived from the target lithologies; shock vaporization and explosive expansion of this water led to the origin of suevites. Below we consider the role of the water in mega disintegration of the Popigai impact melt during cratering.

Water in the Popigai impactites: Our previous studies show that water from target lithologies played an important role at various stages of origin and evolution of the Popigai impact melts: “dry” and “wet” tagamites [1,3]; “dry” and “wet” glass fragments in suevites [3,4]; syngenetic dense water inclusions in lechatelierites [5]; injections of fluid-enriched tagamite melt into the target rocks [6]. A main conclusion resulted from all the studies is that heterogeneous distribution of water inherited by the impact melt from the target lithologies was not homogenized at all the stages of evolution of this melt, including its recrystallization and solidification. The dimension range of these heterogeneities is very broad: from irregular distribution of fluid inclusions and fine alternating of “dry” and “wet” glass bands observed in thin section scale up to alternating of giant, of many hundreds of meters in size, “wet” and “dry” tagamite bodies. We are using this feature in order to explain the nature of mega lump explosive disintegration of the Popigai impact melts.

It is well known that spasmodically heated water, if being closed, shows a high internal pressure. Our esti-

mations for the water inclusions in lechatelierite schlierens from the Popigai impactites show that at the time of solidification of the glasses (temperatures >1700°C) the fluid pressure in the inclusions varied from 0.8-1.5 GPa (a case of gas+liquid inclusions with density ~0.5-0.7 g/cm^3) up to 3.2-3.3 GPa (for entirely liquid water inclusions) [5]. "Exploded" fluid inclusions in lechatelierite are the evidence of a rapid fall of the confining pressure; as a result, the droplets of compressed fluid could not reach the dynamic equilibrium with the host melt by means of a smooth expansion. Behaviors of "dry" impact melt and compressed fluid inclusions inside it are quite different in case of shock pressure release. Thus, the melt unloaded from 50 GPa to atmospheric pressure, increases in volume up to ~2-2.5 times only; at this, the pressure release occurs rapidly, by means of rarefaction waves. In case of the same unloading for the water, the droplet of compressed fluid has to increase its volume to ~2000 times, and has to do a work against viscosity of the enclosing melt. In this case, the pressure release takes place much more slowly, by means of the "piston-like" mechanism. At this, the droplet can explode, if the confining pressure fall was too fast. Anyway, when the confining pressure becomes lower that the fluid pressure inside the inclusion ("X"-moment), this inclusion begins to operate as a local buffer against the pressure fall. So, since the "X"-moment, decompression behavior of a "wet" melt, in contrast to the "dry" one, is determined by expansion of water, as it was found in shock compression experiments on "wet" targets [2].

Origin of the Popigai suevite-tagamite megamixtures: As it was stated above, a complex interfingering of "dry" and "wet" masses represented the bottom centrifugal flow of the Popigai tagamite melts. The "wet" melts kept an excess pressure of water fluid still at the final stages of shock pressure fall by rarefaction waves. That is why, the bands and streams of the "wet" melt could operate as disintegrating or explosive material. As a result of these excess local pressures, the upper part of the tagamite melt flow was disintegrated into large (up to hundreds and thousands of cubic meters in volume) lumps. Turbulent mixing of these lumps with subsiding material of the Parchanai suevite led to origin of the suevite-tagamite megamixtures. Earlier, we partially discussed this mechanism already in [5].

At what part of the melting zone did originate the tagamite melt, affected to mega scale disintegration? Following to data by [2] on the impact melting of water-saturated sedimentary target lithologies, the melt originated in the target volume limited by shock wave isobars 50-100 GPa, was dispersed to ash-like particles; suevites, composed by more large, lapilli-size particles, were derived from the 10 to 50 GPa melting zone. If compared with the scheme, the origin of the Popigai impactites has a number of special features. At first, the Popigai suevites were originated by more complex way than it is supposed by the simple cratering models. At second, the impact melt was derived from the Archean gneisses at shock pressures >50 GPa. However, the scheme proposed by [2] can be accepted in a whole. Following to it, the hottest and partially vaporized melt derived from the central part of the melting zone, was finely dispersed to ash-like particles and deposited either inside the crater (Daldyn suevite formation in the upper part of the suevite strata), or was ejected to outside the crater. Indirectly, the proximal dissemination of the impact melt can be indicated by the strewn field of impact diamonds [1] traced around the Popigai astrobleme to a distance up to 500 km. Less heated melt derived from the next part of the melting zone, was disintegrated to lapilli-size particles and took part in the origin of the PSF. As for the Popigai tagamites, it was earlier noted [1], that based upon complex of their petrographic features, these rocks were derived from the most cold marginal part of the melting zone; it can be inferred that the integrated temperature of the tagamite melts after homogenization of hot spots by thermo-diffusion was lower than the melting points of quartz (~1700°C) and feldspars (~1300-1400°C). We have no objective means to precisely estimate the temperature boundary between the melts which took place in the origin of the PSF, and the melts which formed the tagamites; obviously, the melts affected to mega disintegration, occupied any intermediate position in this sequence.

Similar water-induced (and by other volatiles also) mechanisms of large-scale explosive disintegration of impact melt could take place on the Mars and on the other Solar System planets, and may be of interest in study of large impact structures on these planets.

References: [1] Vishnevsky S. and Montanari A. (1999) GSA Special Paper 339, 19-59; [2] Kieffer S. W. and Simmonds C. H. (1980) Reviews of Geophysics and Space Physics, 18 (1), 143-181; [3] Vishnevsky S. A. (1996) Chemie der Erde, 56, 493-497; [4] Vishnevsky S. A. (1997) LPI Contr. No. 921, 61; [5] Vishnevsky S. A. and Pospelova L. N. (1988) The fluid regime of impactites: dense fluid inclusions in high-silica glasses and their petrologic significance. Novosibirsk, IGG Press, 53 p. (in Russian); [6] Vishnevsky S. A. et al (see abstract submitted to this Nordlingen-2003 Conference).

BRECCIA VEINS, PSEUDOTACHYLITES AND FLUIDIZITE DYKES IN ARCHEAN GNEISS FRAGMENTS FROM THE POPIGAI MEGABRECCIA. S. A. Vishnevsky[1], J. Raitala[2], N. A. Gibsher[1], N. A. Palchik[1], and T. Öhman[2], [1]Institute of Mineralogy & Petrology, Novosibirsk-90, 630090, Russia <nadezhda@uiggm.nsc.ru>; [2]University of Oulu, Oulu, Finland, <jouko.raitala@oulu.fi>.

Introduction: Some Archean gneiss fragments from the Popigai megabreccia exhibit traces of shock metamorphism up to stage II after [1], whereas other gneiss lumps are only fractured and locally brecciated [2]. One of us (S.V.) observed fine-fragment breccia veins with "stream-like" masses of dark cryptograin matter in the lumps; one of the gneiss fragments contains several thin (3-10 cm) dykes filled with tuff-like glass-bearing material. Later it was found that the "stream-like" masses in some breccia veins are pseudotachylites (outcrop No. 479), and dykes with the tuff-like material are injections of impact fluidizites.

Description: *Fine-fragment breccia* of outcrop No. 479 forms linear or branching veins, from first cm to 70 cm thick, in the host biotite-hypersthene gneiss and is made up of psammite-like moderately lithified material. In thin sections, it is a mixture of angular fragments 0.05 mm to 3-5 mm in size, of feldspar, quartz, pyroxene and biotite derived from the parental gneiss, plunged into cryptograin matrix, which composes 15 to 30 % of the rock volume. The breccia contains also submicroscopic bands, of 1-2 mm width and up to 1 cm length, composed by the cryptograin matrix. These bands have no fluidal texture, but form a roughly ordered "stream-like" net in the breccia. Except for the bands, the cryptograin material forms the borders around some gneiss fragments and is present sometimes as clasts in the breccia. No traces of shock metamorphism are found in the gneiss fragments, i.e., shock pressures were <5 GPa at the origin of veins. The breccia is moderately altered and exhibits borders of opaque minerals around some clasts, and cryptograin aggregates of secondary minerals (X-ray data: smectite + traces of chlorite, carbonate and talc). Due to a lack of flowage, the cryptograin bands considered conventionally as ultramilonite.

Fine-fragment breccia with pseudotachylite also forms the veins in outcrop No. 479. It is made up of moderately lithified psammite-like material and is similar to the previous breccia. However, in addition, it contains macroscopic, of 1 to 5 cm width, and up to several dm length, streams and bands of dark-colored cryptograin material. Some of these bands are loose weathered rock; some other are the rocks of moderate hardness. In thin sections, psammite-like breccia is a mixture of angular fragments, 0.05 mm to 3-5 mm in size, of various minerals derived from the parental gneiss with the cryptograin matrix, which composes from 15-20 to 30-40 % of the rock volume. No traces of shock metamorphism are found in the breccia, except for weak and rare kink-bands in biotite. So, the rock originated at shock pressures <5 GPa. The breccia is moderately altered and exhibits borders of opaque minerals around some clasts, and cryptograin aggregates of secondary minerals by places (X-ray data: smectite and traces of chlorite). Loose cryptograin bands did not studied in thin sections and contain smectite + traces of caolinite, chlorite and gypsum (X-ray data). Initially, this material was probably an ultramilonite. Material from the hard bands is fluidal and shows a clear "hump" of amorphous phase on the X-ray diffraction patterns in interval from 19° to 35° ($2\vartheta CuK_\alpha$). That is why, we consider the material as a result of friction melting, i.e., as the pseudotachylite, following to [3]. Alteration of pseudotachylite is represented by calcite and non-maturated smectite; traces of gypsum are also detected (X-ray data).

Impact fluidizites, found in the lump of hypersthene gneiss (outcrop No. 601), are made up of small, from 1-3 mm to 20 mm, particles of the impact glass (from 50 to 70 % of the rock volume) plunged into crystalloclastic matrix represented by fragments, 0.05-3 mm, of the parental gneiss (quartz, feldspar, pyroxene and biotite) and strongly altered cryptograin material. In the most cases, glass particles have fluidal or stream-curved shape, and are "welded" with matrix, i.e., the glass was molten or plastic, when the dykes originated. Highly porous and pumice, strongly altered (X-ray data: smectite + traces of chlorite and dolomite) glasses dominate. Sometimes, the glass is massive and looks like relatively fresh. The glasses contain impurity of troilite-pyrrhotite spherules (1.5 to 40 μ in size); some of them are nickel-bearing or contain the minute inclusions of nickel sulphides (0.7-17.1 wt. % of Ni). Besides it, the spherules, 5 to 33 μ in size, of shock molten and partially decomposed zircon (in wt. %: ZrO_2-66.71; SiO_2-30.81; CaO-0.97; FeO-1.02; total: 99.51) are found in some glasses. Lechatelierite schlierens (97.6-98.8 wt. % of SiO_2) and fragments of diaplectic quartz glass (97.87 wt. % of SiO_2) are present in some glass particles. Gas+liquid fluid inclusions of various densities at 20°C (up to those with dominating of liquid phase, >80 % of the inclusion volume) are present in lechatelierite. Lechatelierite and fused zircon indicate high temperature of the injected

impact melt (>1700°C and ~1800°C, respectively). A bulk geochemistry of the altered glass (72 microprobe analyses) is the next (in wt. %): SiO_2 57.3-70.59; TiO_2 0.31-0.88; Al_2O_3 6.61-16-73; FeO 2.46-7.15; MgO 1.33-4.46; CaO 0.79-3.26; MnO <0.00-0.16; Na_2O 0.61-2.39; K_2O 1.69-3.09; P_2O_5 <0.00-0.14; totals 88.19-96.97. Of average, the glasses are similar to the Popigai tagamites but due to alteration shows the low totals, depletion in Si, Ca and Na, enrichment in Al, Fe, Mg and P; K and Ti are indifferent. A bulk geochemistry of the "fresh" glass (10 microprobe analyses) is the next (in wt. %): SiO_2 59.23-64.16; TiO_2 0.67-1.16; Al_2O_3 14.42-15.96; FeO 5.28-7.94; MgO 3.30-4.80; CaO 2.38-2.85; MnO 0.02-0.18; Na_2O 0.41-1.97; K_2O 2.08-3.02; and totals 91.56-95.60. Of average, the glasses and the Popigai tagamites are very similar to each other.

Gneiss fragments in the rock bear no traces of shock metamorphism, i.e., the dykes originated at shock pressures <5 GPa. Except for the "parental" fragments, small (5-7 mm) rounded clasts of "strange" micro grain dolerite are rarely present in the dykes.

Pumice state of the glasses (in the closed volume of the dykes!), their intensive alteration (in contrast to a fresh state of the host gneiss), mineralogical thermometers (lechatelietite and zircon), and dense fluid inclusions as well show that the tuff-like dyke breccia is a result of dynamic injection of very mobile, hot and fluid-enriched tagamite melt. That is why, we consider the "tuffs" as *the impact fluidizites*. Except for the fluid, the injecting melt contained spherules of liquid iron sulphide. Although the injection of the melt did not provide a shock metamorphism of the host gneiss (lechatelierite, diaplectic quartz glass and spherules of the molten zircon were brought by the melt), nevertheless, the dense fluid inclusions in the lechatelierite indicate a high confining pressure of the melt. In case of the water fluid, following to [4], this pressure at ~1700°C could range from ~0.8-1.5 GPa (gas+liquid inclusions with density 0.5-0.7 g/cm^3) to ~1.9-3.3 GPa (gas+liquid inclusions with density 0.8-1 g/cm^3).

Discussion: Gneiss lumps of outcrop No. 479 with no traces of shock metamorphism were brought from the middle/margin zone of the crater outside the inner ring of Archean gneisses (shock pressures <5 GPa). Their fracturing occurred either at final stages of the shock wave propagation, or at the stage of excavation (colliding in dense turbulent centrifugal bottom flow). Breccia veins show that the gneiss deformation was accompanied by small-scale but fast sliding of the fragments in respect to each other. At this, a part of the material experienced milonitization (*fine-fragment breccia veins*) and friction melting (*breccia veins with pseudotachylites*). Milonite fragments show several stages of brecciation at the origin of the veins.

Fluidizite dykes in the outcrop No. 601 have a specific origin. As in the previous case, the host gneiss lump was brought from the low shock pressure (<5 GPa) zone by means of bottom centrifugal flow. However, at the excavation and transport, it had a dynamic contact with the hot (>1700-1800°C) very mobile and fluid-enriched tagamite melt, which was under the high excess pressure (~0.8-3 GPa in case of water fluid inclusions in lechatelierite). Such pressure could not be lithostatic. We have to conclude that the melt, after its travel from the birthplace to the point of contact with the gneiss lump (not less than 12-15 km), was still under the high residual shock pressure and had large injection ability. It is impossible in case of a fast rarefaction pressure release of the "dry" system. So, we suppose the slow unloading of the melt, as it was found for the "wet" system in shock experiments [5]. Since any moment, a behavior of compressed fluid controls the expansion of the system; "piston"-like expanding, the drops of the fluid work against the melt viscosity and act as the buffer, slowing down the pressure fall [4]. Being under the excess pressure, the fluid-rich melt could inject into the fractured gneiss to a distance not less than 5 to 7 m (a size of the host lump). "Boiling" of the melt took place after the pressure fall. The melt was quenched in "cold" host gneiss, but fused silica glass was still in molten state at the time of injection. Rare clasts of tagamite and silica glass show additional brecciation after the origin of dykes. Then the fluidizites were strongly altered.

Troilite-pyrrhotite Ni-bearing spherules do not exclude contamination of the glass by projectile. We already noted [6], that outer klippen+megabreccia belt in large astroblemes can contain non-eroded portions of the projectile-contaminated impactites. Usually, the meteoritic matter is quickly eroded in large astroblemes, because it is either ejected out, or is deposited at the top of the impact formations inside the crater.

References: [1] Stoffler D. (1971) JGR, 76, 541-551; [2] Vishnevsky S. and Montanari A. (1999) GSA Special Paper 339, 19-59; [3] Reimold W. U. (1995) Earth Sci. Rev., 39, 247-265; [4] Vishnevsky S. A. and Pospelova L. N. (1988) The fluid regime of impactites: dense fluid inclusions in high-silica glasses and their petrologic significance, Novosibirsk, IGG Press, 53 p. (in Russian); [5] Kieffer S. W. and Simmonds C. H. (1980) Rev. of Geophys. and Space Phys., 18 (1), 143-181; [6] Vishnevsky S. A. (1986) In Meteoritc matter and the Earth, Novosibirsk, Nauka Press, 131-159 (in Russian).

EARLY ACCRETION AND DIFFERENTIATION OF PROTOPLANETARY BODIES AND Hf-W CHRONOMETRY

A.V. Vityazev, G.V. Pechernikova, A.G. Bashkirov, Institute for Dynamics of Geospheres RAS, 38 Leninskiy prosp. (bldg.1), 119334 Moscow, Russia,
avit@idg.chph.ras.ru

Introduction. The extinct ^{182}Hf–^{182}W isotope system has been widely applied to date core formation in planetary bodies (e.g., [1]). New Hf–W data for C and H chondrite meteorites [2-4] lead to very rapid accretion and early core formation of asteroids and terrestrial planets: 3–4 Ma for the Vesta, < 30 Ma and < 15 Ma for the Earth and Mars cores formation respectively [2, 3]. According to analytical calculations [5] and computer simulation [6] last stages accretion process of terrestrial planets the value of 100 Ma is preferable. We suggest here other interpretation of new chondritic ratio ^{182}W/^{184}W and the Solar system initial ^{182}Hf/^{180}Hf: these data tell us about initial differentiation in large terrestrial planetesimals and protoplanets at the stage of large impacts before the end of accretion of terrestrial planets. In this scenario Earth's core and Moon were formed later but before late bombardment stage.

Theory and Estimations. Bodies formation in the preplanetary disk was taking place in several stages (see, e.g. [5, 6]). Dust settling and forming of the first generation of planetesimals with the sizes up to 1000 km continued from 1 to 10 Ma. It is ^{26}Al that could be a source of early heating and relative differentiation of the early bodies. Impacts with velocities surpassed 5 km/sec and differentiation of melted interiors were the main sources of energy for heating and differentiation of bodies of sizes above 1000 km which, according to [5, 6], accumulated at times 10–100 Ma (see Table 1).

Heating of a growing protoplanet of mass M while collisions with bodies of mass $m_i = M$ was estimated in [5] as $\bar{T} = T_0 + 1500\text{K}\ (R/1500\ \text{km})^2 f(\mu_i)$, where $f(\mu_i \to 0) \approx 2.5\mu_i$, $f(\mu_i \to 1) \approx 1$. We have the same order of heating by collisions with great number of the less large bodies ($N\ m_j \sim m_i$), namely, $\Delta T_N \sim 1500\text{K}\ N f(\mu_i/N) (R/1500\ \text{km})^2$.

For population of largest planetesimals of the radius R the main characteristic times are
1) accumulation time $\tau_a = R/R' \propto R/(1 - aR^2)$;
2) internal heat transfer time $\tau_\kappa = R^2/\text{Nu}\ \kappa$, (Nu is the Nusselt number accounting the impact stirring as well, $\kappa \approx 10^{-2}$ cm^2/sec);
3) differentiation time $\tau_d = R/v_d$ (v_d is the differentiation velocity).
Possible 3! = 6 regimes are determined by relations of the type $\tau_\kappa < \tau_a < \tau_d$, $\tau_a < \tau_\kappa < \tau_d$ and so on. Two of them are the most interested, they are $\tau_d < \tau_\kappa < \tau_a$ and $\tau_d < \tau_a < \tau_\kappa$. In these cases the differentiation of enough large (1000–3000 km) protoplanet bodies to core and mantle must be accompanied by the additional heating (see Fig. 1).

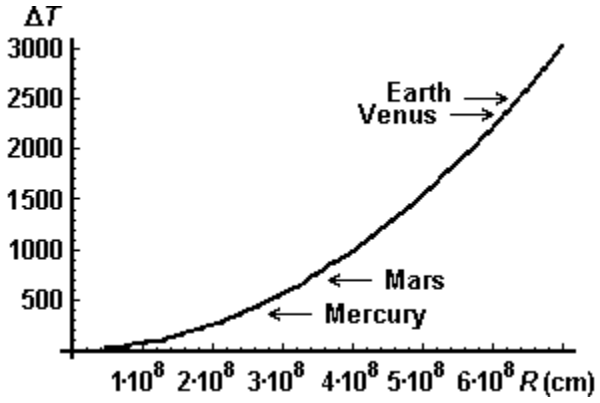

Figure 1: Heating due to gravitation differentiation

With the use of sinking (or sedimentation) equation for the heavy component sinking with the velocity $v_d \propto \exp[-E/R_* T]$ and the heat conduction equation with the source of the form $c\Delta\rho g v_d$, ($g = 4\pi G\ \bar{\rho} R$) we get the criterion for a fast development of the differentiation [5, 7]:
a) $c\Delta\rho g v_{d0} h^2 E/(4\text{Nu}\ \kappa_0\ \bar{\rho} c_p\ R_* T_{d0}^2) > \gamma_{cr}$, $\gamma_{cr} = 0.88$ – flat layer, $\gamma_{cr} = 2$ – spherical layer,
b) $\theta = E\ (T - T_{d0})/R_* T_{d0}^2 > \theta_{cr} \approx 1$.
For characteristic parameters of protoplanets in the terrestrial zone we estimate thickness of the layer where the effective differentiation begins

as ≈ 300 km and find that it depends on these parameters variation weakly.

Discussion. The joint analysis of the planet accumulation at the Large Impact stage and their impact heating up to liquidus temperatures points to essential heating and possible differentiation in exothermal regime with selfheating (between catastrophic collisions). Because of this, Hf – W data can be interpreted as evidence for early differentiation and forming of primitive cores and mantles in large preplanet bodies tens of Ma before their final integration into four terrestrial planets. Data on Nb – Zr [8, 9] evidencing for moderately fast accumulation, and Earth's core formation during 70 – 100 Ma, and presence of relict detrital terrestrial zircons [10] are not in contradiction with this scenario.

Table 1. Typical distribution of the large bodies in the feeding zone of the growing Earth

Mass of the growing Earth $m(t)$	0.7 $m_\oplus$	0.9 $m_\oplus$	0.99 $m_\oplus$
The growth time, 10^6 yr	~ 50	~ 80	~ 100
Masses and radii of five largest bodies			
m_1 (g) r_1 (km)	$3.1\ 10^{26}$ 2600	$1.1\ 10^{26}$ 1900	$1.2\ 10^{25}$ 900
m_2 (g) r_2 (km)	$9.0\ 10^{25}$ 1700	$3.1\ 10^{25}$ 1200	$3.2\ 10^{24}$ 570
m_3 (g) r_3 (km)	$5.1\ 10^{25}$ 1400	$1.8\ 10^{25}$ 1000	$1.8\ 10^{24}$ 470
m_4 (g) r_4 (km)	$3.5\ 10^{25}$ 1300	$1.2\ 10^{25}$ 900	$1.2\ 10^{24}$ 420
m_5 (g) r_5 (km)	$2.6\ 10^{25}$ 1200	$9.0\ 10^{24}$ 800	$9.0\ 10^{23}$ 380
Interval of radii (km)	The number of bodies $N(r)$ in the feeding zone		
500 – 100	2150	870	130
100 – 10	$6.9\ 10^5$	$2.8\ 10^5$	$4.1\ 10^4$
10 – 1	$2.2\ 10^8$	$8.8\ 10^7$	$1.3\ 10^7$

References. [1] Lee, D. C. and A. N. Halliday (1995) *Nature* **378** 771-774, [2] Yin, Q. et al. (2002) *Nature* **418** 949-952, [3] Kleine, T. et al. (2002) *Nature* **418** 952-955, [4] Schoenberg, R. et al. (2002) *Geochim. Cosmochim. Acta* **66** 3151-3160, [5] Vityazev, A. V., G. V. Pechernikova, and V. S. Safronov *Terrestrial Planets* (1990) Moscow Press, [6] Chambers, J. E. (2001) *Icarus* **152** 205-224, [7] Vityazev, A. V. (1980) *PEPI* **22** 289-295, [8] Jacobsen, S. B. and Q. Yin (2001) *LPSC* XXXII, [9] Wade, J. and B. Wood (2001) *Nature* **409** 75-78, [10] Wilde, S. A. et al. (2001) *Nature* **409** 175-178.

LOCALIZED SHOCK EXCURSIONS IN MARTIAN METEORITES: THE LOS ANGELES BASALTIC SHERGOTTITE AND NORTH WEST AFRICA 1183 OLIVINE-PHYRIC SHERGOTTITE. E.L. Walton[1] and J.G. Spray, Planetary and Space Science Centre, Department of Geology, University of New Brunswick, 2 Bailey Drive, Fredericton, New Brunswick E3B 5A3, Canada. [1]Correspondence author's e-mail address: j5rng@unb.ca

Introduction: Shock waves are produced naturally by the hypervelocity impact of extraterrestrial bodies. The resultant shock metamorphic effects are a feature common to all meteorites (*e.g.,* chondrites, irons, achondrites, SNCs). It is imperative to have a complete understanding of the effects of shock on the SNCs, as these features reflect normal geological processing by impact of material on the Martian surface. The Los Angeles and NWA1183 meteorites have not undergone any detailed studies of their shock metamorphic effects, despite the presence of localized shock excursions manifest as discrete melt pockets, veins and dikelets. As such, this study is devoted to the characterization and description of shock metamorphic effects using analytical electron microscopy, as recorded in the NWA1183 and Los Angeles shergottites.

Method: One large thick section of NWA1183 (1.86 g: ~ 2.1 cm x 1.9 cm x 0.3 cm) and two round thin sections of Los Angeles stone 1 (sections LA 7058-2; 2.1 cm x 1.2 cm, LA 7058-5; 1.3 cm x 1 cm) were initially studied using optical microscopy (reflected light for NWA, transmitted and reflected light for LA). Areas of interest (localized shock melting) were further investigated using a JEOL 6400 digital scanning electron microscope. SEM backscattered electron (BSE) imagery was used to investigate the microstructures and mineralogy of both meteorites. Defocussed beam microprobe analysis was deployed to determine the approximate bulk chemistry of melt pockets within Los Angeles.

NWA1183: A large mass of 522 g and twenty two additional fragments, having a combined weight of 576.77g, were found in 2001 in the Maarir region near the border of Morocco and Algeria [1]. NWA1183 is an olivine-phyric Martian basalt paired with this find (NWA1068/1110). NWA1183 has a porphyritic texture consisting of olivine phenocrysts (generally < 2.5 mm) embedded in a fine-grained groundmass of euhedral to subhedral pyroxenes (pigeonite and augite) and interstitial plagioclase (now maskelynite).

Localized shock-induced melting. Areas of localized shock-induced melting include discrete melt pockets and shock veins. Their shock metamorphic nature is revealed by a crosscutting relationship with host rock igneous textures. In hand specimen, shock veins are readily visible forming an interlocking network of black glassy veins that transect the sample. Only one set of shock veins have been observed. They have variable thickness ranging from 1 μm to 100 μm, largely defined by the remobilization of sulfides, and melting and incomplete mixing of host rock minerals (plagioclase, pyroxenes, olivine) forming flow-textured schlieren. Offsets along the shock veins (*e.g.*, dextral sense of displacement on the order of 60 μm observed for one olivine phenocryst) indicate that the veins are essentially formed by frictional melting, in analogy to the formation of micro-pseudotachylytes in shocked rocks of terrestrial impact craters [2]. Melt pockets comprise <5 % of the meteorite by volume, ranging from <0.5 mm to 6 mm in apparent diameter. They are heterogeneously distributed throughout the sample having microcrystalline groundmasses with rapid growth textures (feather, skeletal and dendritic crystal morphologies). Host rock minerals (olivine, pyroxenes) adjacent to the melt pockets contain planar fractures that occur only on the side of the grain in direct contact with the melt. Small (<5 μm-sized) pyroxene clasts have, in rare cases, been observed within the shock veins that do not contain any fractures. They have subrounded, or less often, euhedral to subhedral grain shapes. Rounded to spherical blebs of immiscible sulfides are abundant within the melt products, a morphology typical for those sulfides in shock- produced melts [3]. Host rock plagioclase has been converted to maskelynite having irregular fractures radiating from grain boundaries into adjacent minerals (volume increase upon melting).

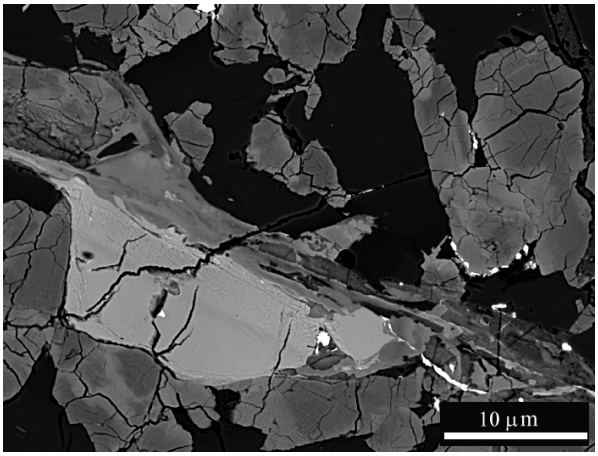

Fig.1. BSE image of a shock vein within NWA1183 (top left to bottom right) truncating an olivine phenocryst (lightest greyscale).

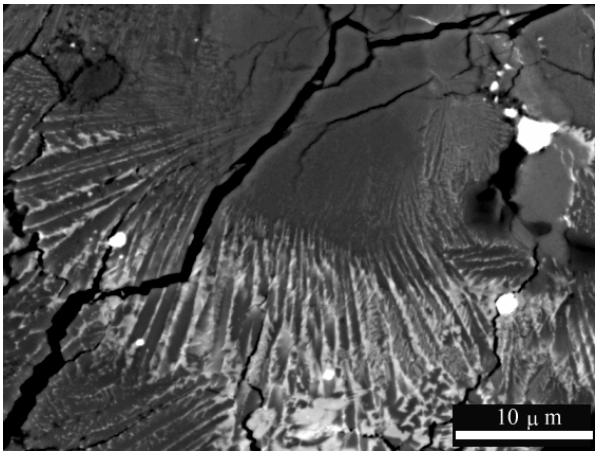

Fig. 2. BSE image of a typical shock melt within NWA 1183 showing rapid growth textures attributed to rapid cooling (quenching).

Los Angeles: Localized regions of melting comprise <3 % of the meteorite by volume, forming three discrete type of melt zones (0.07 x 1.3 mm – 3.0 mm x 3.5 mm) possessing glassy to microcrystalline groundmasses. These melt pockets are differentiated on the basis of size, clast volume and degree of crystallization and vesiculation. Melt pockets and melt dikelets emanate from the melt pockets up to 3 mm into the host rock, but do not necessarily connect with other melt pockets. The overall bulk composition of the melt pockets is dependent on those minerals that are in direct contact with the melt pocket The melt pockets were generated by pressure-temperature excursions of 60-80 GPa and 1600 – 1800^{o}C by the *in situ* melting of host rock minerals. Unlike those observed in NWA1183, melt veins and melt dikelets in LA 7058 are considered morphologically distinct (within the two dimensions of the thin section) from typical 'shock veins' that transect the NWA1183.

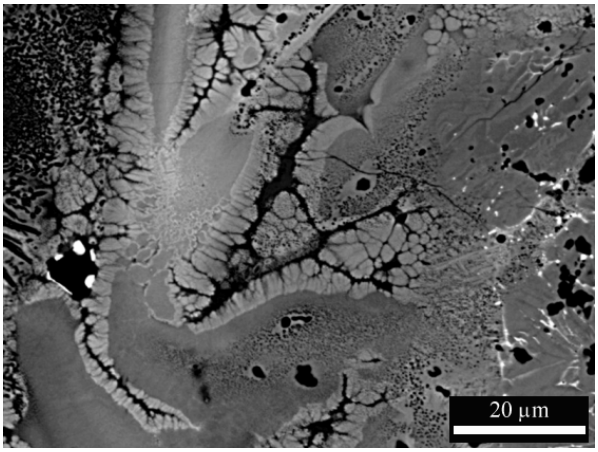

Fig. 3. BSE image showing the extreme heterogeneity of microtextures in the melt pockets.

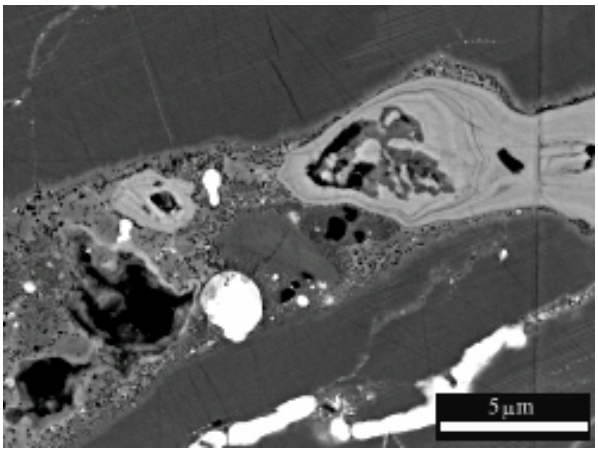

Fig. 4. BSE image of a 'melt vein' in LA 7058-5. The melt vein crosscuts a host rock pyroxene extending <1.2 mm distance from the melt pocket from which it emanates.

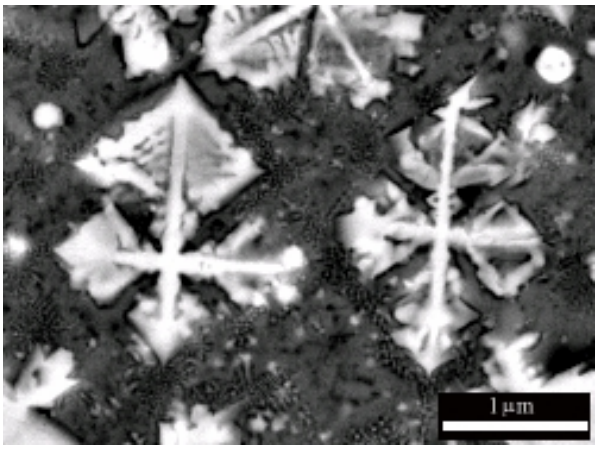

Fig. 4. BSE image of dendritic titanomagnetite crystals within a melt pocket in LA 7058-2.

References: [1] Barrat et al. (2002) *Geochim. Cosmochim. Acta, 66*, 3505-3518. [2] Spray (1998) *Geol. Soc. London Spec. Pub.*, *140*, 195-204. [3] Stœffler et al. (1991) *Geochim. Cosmochim. Acta, 55*, 3845.

Acknowledgements: This work has been funded by the Natural Sciences and Engineering Research Council of Canada through a PGS-B grant awarded to ELW. The authors also acknowledge generous student travel support provided by The Barringer Crater Company.

LUNAR PROSPECTOR DATA IMPLY AN AGE OF 4.1 GA FOR THE NECTARIS BASIN, AND OTHER PROBLEMS WITH THE LUNAR "CATACLYSM" HYPOTHESIS P. H. Warren, Institute of Geophysics, UCLA, Los Angeles CA 90095-1567, USA (pwarren@ucla.edu).

Lunar polymict impactite samples have yielded ages that are remarkably clustered near 3.9 Ga, especially for impact melt breccias. This curiously unimodal age spectrum represents one of the most profound discoveries of planetary sample research. It clearly indicates that the rate of cratering (i.e., collisions between the Moon and asteroids and comets) was vastly higher ~3.9 billion years ago than it has been over the last 85% of solar system history. The bombardment history before 3.9 Ga has been most controversial. The relative scarcity of ages >3.9 Ga has led many, in recent years most notably Ryder [e.g., 1,2] to infer a spike in the global lunar cratering rate at ~3.9 Ga. Following Tera et al. [3], this cratering spike concept is somewhat confusingly known as the lunar "cataclysm" hypothesis. A broader, generally accepted hypothesis known as "late heavy bombardment" simply postulates vastly higher, more destructive lunar cratering at ~3.9 Ga, without regard to the spike question. The controversy concerns the degree to which the clustered ~3.9 Ga ages reflect a large-factor and global spike, as opposed to a bump or inflection on a basically monotonic decline in the late-accretionary impact rate.

A key datum in this debate is the inferred age of the Nectaris basin. On photogeologic-stratigraphic grounds, Nectaris is clearly older than Imbrium and Serenitatis; and two-thirds (30 out of 44) of the Moon's still recognizable basins appear even older than Nectaris [4]. Impact melt breccias of Nectaris origin are presumably present among the Apollo 16 samples, acquired ~550 km from the center of Nectaris. Ar ages for Apollo 16 impact melt breccias mostly cluster from 3.87-3.92 Ga, and 3.90-3.92 Ga has become almost canonical as the age of Nectaris [e.g., 4,5]. But as Korotev et al. [6] have noted, the absolute age of Nectaris is unclear.

Lunar Prospector results [e.g., 7,8] indicate a remarkable global-scale heterogeneityin the the concentrations of incompatible elements; these elements are much lower in the broad region of Nectaris,SE of the Apollo 16 site, than in the regions to the N and W where the other basins that potentially contributed impact melt breccias to the Apollo 16 megaregolith. It is instructive, therefore, to compare the ages of Apollo 16 impact melts vs. their contents of incompatible elements. Fig. 1 shows such a comparison, using the frequently determined element K. The data are far from random. The impact melts with low K (filled symbols: K < 430 μg/g) that are most plausibly linked with Nectaris tend to be close to 4.1 Ga. This distribution severely militates against the common interpretation [e.g., 2] that the age of Nectaris is ~3.90 Ga.

The ages of the Imbrium and Serenitatis basins are probably 3.85-3.9 Ga [e.g., 2]. The age of a fourth lunar basin, Crisium, can in principle be constrained using Luna 20 samples. On photogeologic-stratigraphic grounds, Crisium appears similar in age to Serenitatis, i.e., older than Imbrium but younger than Nectaris [4]. Cohen et al. [9] obtained Ar ages for six Luna 20 rocklets and reviewed literature data for 12 others. Swindle et al. [10] found a loose clustering of ages at 3.75-3.90 Ga. Swindle et al. [10] suggested (in a "tentative" way) that the oldest sample in this cluster, 3.895±0.017 Ga, might date the Crisium impact. However, it is not even clear the sample in question is an impact melt breccia (no thin section was made). Also, among the samples dated by Cohen et al. [9], most are in this author's opinion probably either impact melt breccias or annealed impact melt breccias (genuine, pristine "gabbros" seldom have grain sizes of <200 μm like rocklet 2004D; pristine troctolites seldom have grain sizes of <100 μm like rocklet 2004C). Considering all of the 13 or so Luna 20 rocklets that have yielded Ar ages (review: [9]) and are likely impact melt breccias, the data (excluding the 0.52 Ga outlier) show an almost even distribution across the range 3.75-4.19 Ga. In other words, the age of the Crisium impact is not yet constrained beyond being probably within the range 3.8-4.2 Ga. For these and other reasons, the validity of the lunar cataclysm hypothesis remains very much in question.

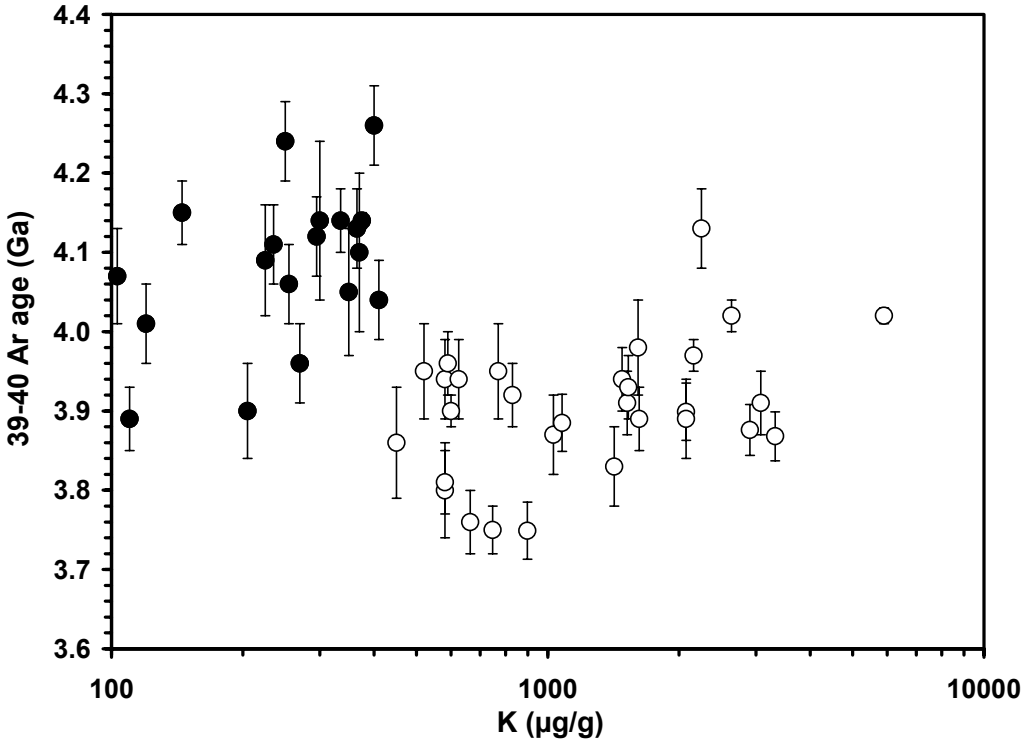

Fig. 1. Bulk-rock potassium vs. ^{39}Ar-^{40}Ar age for 50 Apollo 16 impact melt breccias. Literature data were taken from a variety of sources, most notably Dalrymple et al. [5], and other sources compiled by James [11]. Filled symbols: K < 430 µg/g.

References: [1] Ryder G. (1990) *Eos* 71, 313-323. [2] Ryder G. (2002) *JGRP* 107, No, E4-6. [3] Tera F. et al. (1973) *LPS IV*. [4] Wilhelms D. E. (1987) *The Geologic History of the Moon* (USGS Prof. Paper 1348), 302 p. [5] Dalrymple G. B. *LPS* 32, abstract #1225. [6] Korotev R. L. et al. (2002) *Workshop on the Moon and Beyond*, abstract #3029. [7] Lawrence et al. (1998) *Science* 281, 1484-1489. [8] Prettyman et al. (2002) *LPS* 33, abstract #2012. [9] Cohen B. A. et al. (2001) *MaPS* 36, 1345-1366. [10] Swindle T. D et al. (1991) *Proc. Lunar Planet. Sci.* 21, 167-181. [11] James O. B. (1981) PLPSC 12, 209-233.

OCEANIC IMPACTS, TSUNAMIS, AND THE INFLUENCE OF THE WATER DEPTH ON THE QUANTITY AND CHARACTERISTICS OF THE GENERATED WAVES. R. Weiß[1], K. Wünnemann[2], H. Bahlburg[1], [1]Geologisch-Paläontologisches Institut und Museum, Westfälische Wilhelms Universität–Münster. Corrensstraße 24, 48149 Münster, Germany; [2]Department of Earth Science and Engineering, Imperial College London, London SW7 2AZ, United Kingdom (robweisz@uni-muenster.de, k.wunnemann@ic.ac.uk)

Introduction: The probability of an oceanic impact is three times larger than the impact of an asteriod on continents. Nevertheless most known impact craters are on land. The apparent lack of oceanic impact structures is mainly caused by two reasons: (1) The oceanic crust is being subducted which means that potential impact craters have disappeared. (2) If the impactor is not large enough (too less kinetic energy) to reach the ocean bottom, no crater structures are left behind. In contrast, each impactor, that hits any continental site of the earth surface, produces an impact crater.

Numerical experiments, carried out by Artemiva & Shuvalov [1], showed that the ratio between the water depth H and diameter of the impactor d has to be larger than 0.1 to generate a typical impact structure on the ocean bottom. If the H/d ratio is between 0.1 and 1, the water column has a strong influence on the impact cratering processes. Shuvalov et al. [2] and Gault and Sonett [3] showed that the morphology of oceanic crater structures differs from those on continents.

If the H/d ratio decreases, the influence of the water column also declines. For an H/d ratio less than 0.1, the water column does no longer affect the cratering processes itself. Such impacts might be simulated as solid earth impacts.

Nevertheless, tsunamis are transmitted from the impact point, even if the H/d ratio is very small. Generally, the generated tsunami waves can be subdivided into two classes: (1) The first class is represented by the rim wave, which is induced by the collapse of the crater rim and ejecta curtain during the excavation of the crater. (2) The second class, referred to as collapse waves, is caused by the collapsing cavity in the water. The H/d ratio has a clear influence on the characteristics of each transmitted tsunami wave. It is reasonable that the number of the transmitted tsunami waves also depends on the H/d ratio. For example, if the impactor does not reach the ocean bottom, the collapse of the cavity causes free oscillation of the water column and a large number of collapse waves are generated. If the H/d ratio is small, the number of transmitted tsunami waves is strongly limited. If the crater rim is slightly higher than the original water depth, the water cannot powerfully resurge into the crater to generate the collapse wave. In this case, the rim wave is the only wave that propagates outward from the point of impact.

This study focuses on the variation of the quantity and the characteristics of transmitted tsunami waves due to an oceanic impact. To attain the goal, we are utilising different numerical models, which compute the impact process and the wave propagation. The impact model is used to calculate the initial conditions (the number of tsunami waves and their characteristics) for the wave propagation model, by varying the H/d ratio. The computation of the wave propagation allows to study the change of the wave characteristics during the propagation over an artificial bathmymetry.

Generation of Tsunami Waves: The impact process is calculated by an extended version [4] of the well-established SALE Hydrocode [5]. Because of large deformations during the impact, all computations have to be done in pure Eulerian mode. The 2-D geometric model, including the water column, was constructed using a non-uniform computational grid that consists of 400x450 cells, with a minimum cell size of 25m. The projectile is 1km in diameter (corresponds to 40 cells) and hits the ocean surface at 12km/s. For this study, the water depth is varied between 250m (10 cells) and 1250m (50 cells) which corresponds to a variation in the H/d ratio from 0.25 to 1.25. Fig. 1 shows a series of snapshots, sketching the generation of the rim wave and the collapse wave. For this case the H/d ratio is 1.25.

Propagation of Tsunami Waves: The hydrodynamical background of the wave propagation model is the shallow water approach. This approach assumes that the length of a wave is much larger than the water depth. Tsunamis fulfil this assumption. The shallow water approach can be derived by an integration of the Navier-Stokes equation performed for the depth coordinate. The present work is based on a non-linear version of the shallow water approach, consisting of adjustment and advection.

The equations of the shallow water approach are seen as a classic “2+1” problem [6]. “2” represents the two orthogonal space directions, and “1” is the time. To solve this problem, we are using centered finite difference scheme. Fig. 2 gives the graphical representation of the numerical scheme and the applied operators. In this scheme, a parameter in point $P(x,y,t+\Delta t)$ depends on the neighbouring points $P(x+1,y,t)$, $P(x-1,y,t)$, $P(x,y+1,t)$ and $P(x,y-1,t)$ and on the point itself $P(x,y,t)$ in the previous time level.

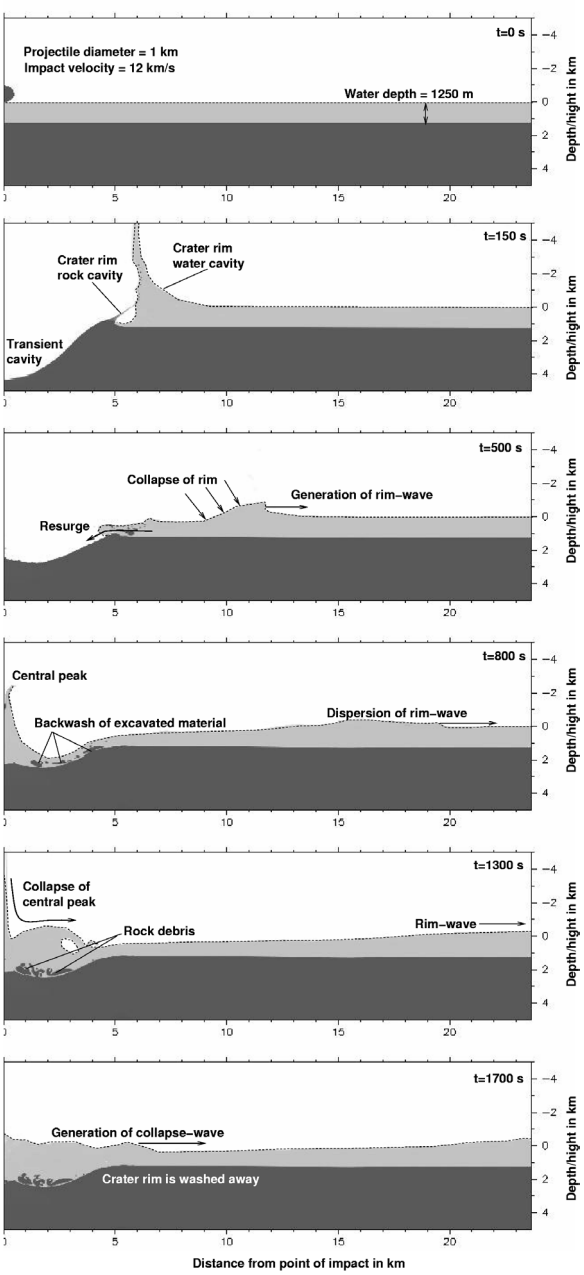

Figure 1: Snapshots of different stages of the generation of the rim and the collapse wave by an oceanic impact.

The calculations remain stable as long as ($c(\Delta x+\Delta y)/\Delta t<1$. c is the group velocity of tsunami waves. A further important step was to apply the LAX operator of the parameters at point P(x,y,t) to make the numerical scheme more stable. The implementation of the LAX operator allows to run the wave propagation model without an additional diffusion term.

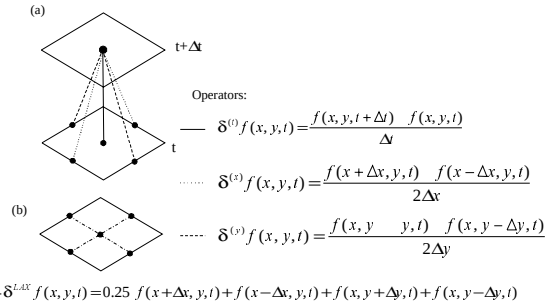

Figure 2: Graphical representation of the used numerical operators

Conclusion: The simulations of oceanic impacts with varying water depth show that the number of generated waves is strongly affected by the H/d ratio. If the H/d ratios is less than 1.0 the rim wave will be the only one that is generated by the impact. For larger ratios, further waves are induced by the back surge of the water into the crater. The impact model suggests already, that the rim wave underlies strong dispersion (Fig 1, t=800 s). Modelling the wave propagation allows to quantify the effect of dispersion especially if the bathymetry changes. The models show that the rim-wave can only survive over longer distances if it runs into a bathymetric deepening. If the water depth remains constant, the rim wave will disappear by dispersion.

References:

[1] Artemeiva N. A., Shuvalov V. V. (2002), *DSR II, 49, 959-965.* [2] Shuvalov V.V, Dypvik H., Tsikalas F. (2002) *JGS, 107,xxx-xxx*. [3] Gault D. E., Sonett C. P. (1982), *Spec. Pap. Geol. Soc. Am., 190, 69-92*. [4] Wünnemann K., Lange M. A. (2002) *DSR II, 49, 969-981* [5] Amsden A. et al. (1980), Los Alamos National Laboratory Report LA-8095, Los Alamos, 101pp. [6] Titov V. V., Synolakis C. E. (1997*), GRL, 24, 1315-1318*.

THE DEPENDENCE OF TARGET PROPERTIES UPON FRESH CRATER MORPHOLOGIES ON MARS. J. Whitehead[1], R. A. F. Grieve[2], J. B. Garvin[3] and J. G. Spray[1]. [1]Planetary and Space Science Centre, Department of Geology, University of New Brunswick, 2 Bailey Drive, Fredericton, New Brunswick, E3B 5A3, Canada, jwhitehe@unb.ca, [2]Earth Sciences Sector, Natural Resources Canada, Ottawa, ON, K1A OE4, Canada. [3]NASA Headquarters, Office of Space Science, Washington DC, U.S.A.

Introduction:

Viking and Mars Orbiter Camera (MOC) images for ~900 "fresh" complex craters were chosen for inspection from a database of 1599 complex craters for which physical attributes have been obtained using the Mars Orbiter Laser Altimeter (MOLA) [1]. Preliminary analysis revealed that many of the complex craters have been significantly modified by various processes of denudation, as well as partial or complete infilling with sediments ± impact melt ± lava [2], considerably shallowing many of the craters. This study confirms that the majority of the 894 sampled complex craters are affected by such processes. In 474 cases (52%), no central peaks were observed owing to erosion or burial. Of the remaining craters with visible central peaks, 159 of the freshest craters were selected for further study. These were chosen based on: the absence of significant infilling materials; the presence of a sharp rim and, typically; the preservation of the finer scale morphologic features of the associated ejecta blanket. These craters were used in order to assess the association between the target type and various central peak morphologies, ejecta types and crater depth/diameter relations.

The average depth/rim crest diameter (d/Drc) value for the freshest craters without a large apparent impact melt sheet is 0.062 ± 0.040 (n=152, 2σ). Fresh craters containing significant impact melt possess an average d/Drc value of 0.038 ± 0.036 (n=7, 2σ) which is not significantly different from the average d/Drc value for the degraded and/or partly filled complex craters (0.041 ± 0.040 (n=735, 2σ). 92% of the freshest craters are <40 km in diameter, whereas only 58% of the degraded craters possess Drc values <40 km, indicative of the average older age of the larger crater population.

A target type for each fresh crater was recorded using the photo-geologic interpretations of [3, 4, 5]. Target types were defined with the aim of separating targets with inferred different strengths. These types comprise, from weakest to strongest: breccia and or sediment; breccias/sediment with interlayered volcanic flows; volcanic flows with overlying aeolian deposits, and; volcanic flows alone. There is no correlation between the rim crest diameter-normalised central peak widths (Dcp/Drc) and the target type (correlation factor, c.f. of -0.084). In addition, there is no correlation between the d/Drc ratio and the target type (c.f., -0.081). This indicates that either the crater morphologies are insensitive to target type or that the surface geologic interpretations do not accurately reflect the target strengths at depth.

The geometry of lunar central peaks has been shown to be sensitive to target type, with linear central peaks being more commonly present on the highland terrain than on the mare [6]. On Mars, the central peak geometry also appears to be dependent on the target type, with linear peaks being slightly more common on targets comprising sediments and breccias (26%) as compared to volcanic flow-dominated targets (20%) (n=130 fresh craters).

The central peaks can form one contiguous uplift, or can comprise several isolated topographic highs. As on the moon [6], the contiguousness of the central peaks for the fresh Martian craters appears to be independent of the inferred strength of the target.

The Martian central peak widths are related to the rim crest diameters according to the following relation $Dcp = 0.16Drc^{1.20}$. The analogous relation for 172 fresh lunar craters, calculated using data generously supplied by Wendy Hale, is $Dcp = 0.17Drc^{1.05}$[6]. The lower power law function for the lunar craters indicates that, for a given crater diameter, wider central peaks are generated on Mars than the moon. This may be related to target differences between these bodies and/or the higher gravity of Mars.

References: [1] Garvin J. B. et al. (in preparation), *to be submitted to JGR, Planets.* [2] Whitehead J. et al. (2002) *MAPS 37(7),* A150. [3] Scott D.H. and Tanaka, K.L. (1986), *U.S.G.S. Misc. Investig. Series, Map I_1802_A.* [4] Greely R. and Guest, J. E. (1987) *U.S.G.S, Misc. Investig. Series, Map I_1802_B.* [5] Tanaka K.L. and Scott D.H. (1987) *U.S.G.S. Misc. Investig. Series, Map I_1802_C.* [6] Hale, W. and Head, J.W. (1979) *Proc. 10th LPSC,* 2623-2633.

STRUCTURAL AND GEOCHRONOLOGIC CONSTRAINTS ON THE TIMING OF THE CHARLEVOIX IMPACT, QUEBEC, CANADA. J. Whitehead[1], S. Kelley[2], S.C. Sherlock[2], R. A. F. Grieve[3], J. G. Spray[1], and C. A. Trepmann[1]. [1]Planetary and Space Science Centre, Department of Geology, University of New Brunswick, 2 Bailey Drive, Fredericton, New Brunswick, E3B 5A3, Canada, jwhitehe@unb.ca, [2]Department of Earth Sciences, The Open University, Walton Hall, Milton Keynes MK7 6AA, UK., [3]Earth Sciences Sector, Natural Resources Canada, Ottawa, ON, K1A OE4, Canada.

Introduction: Accurate determinations of the ages of impact structures are required if associations between impacts and extinction events are to be tested. In addition, the extistence of multiple and potentially related impacts can only be inferred if accurate ages exist for the candidate impacts.

Although the 54 km-diameter Charlevoix impact structure in Quebec, Canada (47°32' N, 70°17' W) is the 13th largest confirmed impact structure on Earth [1] its age is poorly constrained.A potential association between an impact event and the Devonian Frasnian/Famennian extinction has been made [2], and Charlevoix is a natural candidate. However, the established Devonian K-Ar ages for Charlevoix are inconsistent with the outcrop pattern of the structure. Here we present the preliminary results of a new Ar-Ar dating study of impact melt rocks and pseudotachylytes from the structure.

Existing Age Constraints: Precambrian anorthosites, charnockites and granitic gneisses in the target rock are overlain by the Ordovician Black River, Trenton and Utica Groups – constraining the impact event to Ordovician or post-Ordovician times.

The north-western limit of Appalachian thrusting, Logan's line, truncates the southeastern margin of the crater in the St Lawrence River. This fault clearly accommodates post-impact movement juxtaposing the impact structure with unshocked rocks to the immediate southeast on the Isle aux Coudres. If this post-impact thrusting is a result of Taconic to Salinic orogenesis (Ordovician to upper Silurian), then the impact occurred during the Ordovician or early Silurian, not the Devonian.

The existing K-Ar ages for impact melt rocks (342 and 372 Ma) and pseudotachylyte (335 Ma) from the structure [3] were determined prior to the 1977 publication of a standardised set of decay constants by Steiger and Jäger [4]. Despite this, the recalculated ages (327, 356 and 321 Ma, respectively) are seldom presented in the literature – and no longer are contemporaneous with the Frasnian-Famennian extinction.

The quoting of uncorrected ages is not restricted to the Charlevoix impact – here we present the recalculated ages of six other craters whose ages were determined prior to 1977 (Table 1).

The age of impact events are typically best determined by the isotopic ages of impact melt rocks. At Charlevoix, the two melt rock ages, which were obtained by two separate labs, differ by 31 Ma [3]. Owing to the range of these ages, the timing of the impact has been variously quoted as an average of these two ages [5] or as the younger age, on the basis that the younger sample may have experienced a partial resetting of the isotopic system, possibly as a result of subsequent tectonic activity or devitrification of groundmass glasses.

Table 1

Structure	Reported Age (Ma)*	Method	Lithology	Recalc. age (Ma)**
Aouelloul, Mauritania	3.1 ± 0.3	K-Ar	glassy impact melt	3.0 ± 0.3
Brent, Canada	≥ 414 ± 20 450 ± 9	K-Ar Ar-Ar	impact melt impact melt	≥ 396 ± 20 431 ± 9
Charlevoix, Canada	342 † 372 † 335 †	K-Ar K-Ar K-Ar	impact melt impact melt pseudotachylyte	327 356 321
Ilyinets, Ukraine	395 ± 5	K-Ar	impact melt	378 ± 5
Steen River, Canada	95 ± 7	K-Ar & Rb-Sr	pyroclastic whole rock	91 ± 7
Tenoumer, Mauritania	2.5 ± 0.5	K-Ar	impact melt	2.4 ± 0.5
Wanapitei, Canada	37.8 ± 1.6 36.0 ± 1.6	K-Ar K-Ar Ar-Ar	glass whole rock †† impact melt	36.2 ± 1.6 37.2 ± 1.2

* Ages calculated using pre-1977 decay constants.
** Ages recalculated using decay constants of Steiger and Jäger, 1977
† no errors reported
†† glass is undevitrified and whole rock is partially devitrified

The degree of partial resetting of ages by post-impact heating or disturbance by St Lawrence faulting and fluid flow is unknown, though the impact melt rocks and pseudotachylytes are both highly susceptible to resetting owing to their fine grain sizes.

Sample Descriptions: Samples dated at the Open University, UK include three *in situ,* and two potentially glacially displaced impact melt rocks, and one pseudotachylyte from the central uplift.

Three of the impact rock samples possess a cryptocrystalline groundmass of quartz, andesine, albite and orthoclase, ilmenite and titanite surrounding acicular crystallites of augite, ranging from 0.2 to 14 mm long, with widths typically <20 μm.

One impact melt rock collected from glacial till possesses a coarser groundmass grain size than the in-situ samples with crystals of 10-400 um in diameter. Groundmass phases include quartz, titanite, alkali feldspar (10-20 μm) and secondary clinochlore. The sample also contains lechatelierite glass with flow texture and shocked, toasted quartz [6].

The pseudotachylyte sample was taken from a vein within central peak anorthosites and has a uniform grain size of 1-5 μm, and contains clasts of anorthosite. X-ray compositional maps indicate that the K is distributed evenly throughout the matrix.

New Age Data: The samples were analysed by melting spots ~ 100 μm in diameter using a focused laser, a technique which highlights age variations within the sample. Approximately 60 laser spots were

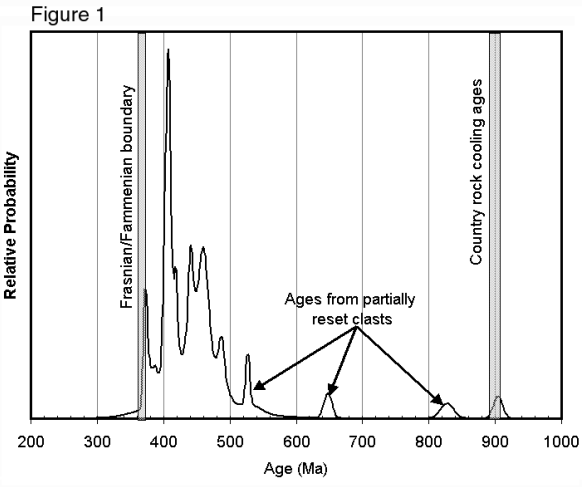

analysed, yielding individual spot ages ranging from 356 Ma to 904 Ma (Figure 1). All spot ages older than 500 Ma are associated with above average Ca/K values (calculated from the $^{37}Ar/^{39}Ar$ ratios) and are the same age or younger than local country rock cooling ages (around 900 Ma). It seems likely that these ages are influenced by clasts either partially reset or mixed with younger melt material in the analysis. All but one of the remaining spot ages are all older than 370 Ma (the Frasnian/Famennian boundary is generally thought to be at 364 Ma, see Figure 1) and thus the Ar-Ar data confirm field observations and indicate that the Charlevoix impact did not occur at the Frasnian/Famennian boundary.

The other peaks in age are sometimes attributable to one sample, for example all ages in the peak at 375 Ma result from one sample (4 analyses) and two samples dominate the age peak around 410 Ma. However, all samples show some peaks in the range 450-480 Ma and two of the three *in situ* melt rocks yield age spectra peaking in the range 460 to 470 Ma (the other yielded more scattered ages). Unfortunately the low potassium and high calcium content of the pseudotachylyte prevented high precision ages being determined.

The best constraint upon the age of a resetting event might be cooling from the Acadian orogeny, which has been dated in slightly higher grade rocks some 200-250 km further south at 377 ± 4 Ma [7]. It seems likely that the low grade metamorphism affected the glassy and fine grained rocks of the Charlevoix impact leading to young K-Ar ages. The Ar-Ar samples of the present study avoid some of the later alteration effects. However, the preliminary Ar-Ar data clearly indicate a complicated age pattern, but one which seems to corroborate the field data and indicates that an Ordovcian impact in the age range 450-480 Ma, probably close to 460-470 Ma. Identifying the precise impact age seems to be hampered by later low grade metamorphism and thrusting, which have caused partial argon loss during heating and alteration of the primary mineral and glass assemblage. Further work will be undertaken, including step heating selected samples and further sample collection, to obtain a better constraint on the age of the impact.

Conclusions: The Charlevoix impact is not Devonian, as indicated both by field data and new Ar-Ar ages. The impact was probably Ordovician (Llanvirn using the timescale of [8]). Scattering of the ages has been caused by later thrusting, low grade metamorphism and fault movements coupled with various degrees of excess argon from the target rocks. The three previously published K-Ar ages [3] will also have been disturbed by these factors and therefore are of limited use.

The association between the Charlevoix impact event and the Frasnian/Famennian extinction event is no longer tenable. However, if the Charlevoix impact was generated approximately 460 to 470 Ma ago then it may have been broadly contemporaneous with the Ames, Granby and Neugrund structures in Oklahoma, Sweden and Estonia, respectively. In addition, a high flux of potentially coincident meteorites has recently been reported for the Orodovician [9]. Despite the coincidence of these events with the probable new age for Charlevoix, no genetic association should be made until the isotopic age of Charlevoix is further refined.

References: [1] Earth Impact Database, 2003. <www.unb.ca/passc/ImpactDatabase/>(Accessed: 11th May, 2003). [2] McLaren D. (1970) *J. Palaeont, 44,* 801-815. [3] Rondot J. (1971) *JGR, 76,* 5414-5423. [4] Steiger R.H. and Jäger E. (1977) *EPSL, 36,* 359-362. [5] Grieve R. A. F. et al. (1995). *GSA Today, 5*, 193-196. [6] Whitehead J. et al (2002) *Geology, 30,* 431-434. [7] Whitehead J. et al (1996) *Geology 24*, 359-362. [8] Gradstein F. M and Ogg J. (1996) *Episodes,19*, 3-5. [9] Schmitz B. et al. (2003) *Science, 300,* 961-964.

CHRONOLOGY OF IMPACT-RELATED DEFORMATION IN THE CENTRAL UPLIFT OF THE VREDEFORT IMPACT STRUCTURE, SOUTH AFRICA. F. Wieland, wielanf@science.pg.wits.ac.za, R.L. Gibson, W.U. Reimold, and C. Lana, Impact Cratering Research Group, School of Geosciences, University of the Witwatersrand, Private Bag 3, P.O. Wits 2050, Johannesburg.

Summary:. This study presents results of a structural investigation of the inner parts of the central uplift of the Vredefort impact structure. A 20-25 km thick crustal section has been rotated on-end to form the central uplift, which displays evidence of increasing shock deformation towards the center of the dome. The dome possesses a polygonal geometry, with the polygon segments separated by zones of asymmetric folding and radial oblique-slip faulting. The strong orientation asymmetry in the northwestern and southeastern parts is attributed to a dipping pre-impact sequence. Multiple joint sets are intensely developed in all rock types and display predominantly normal-slip displacements, consistent with radial and tangential collapse of the central uplift. These joints may postdate shock-related pseudotachylitic breccia veins, although the latter commonly appear to have crystallized only after joint formation.

Introduction: The 2.02 Ga, ca. 300-km-wide Vredefort impact structure in South Africa is one of the largest impact structures on Earth [1]. Between 7 and 10 km of erosion has led to the removal of the crater and its impact breccia fill, and has exposed the deep levels of the structure. The present study is focused on the northern and western sectors of the collar, in rocks of the 2.71-2.98 Ga Witwatersrand Supergroup. These rocks form the innermost collar, at a radial distance of ~20-30 km from the center of the dome, and have been uplifted by at least 15 km relative to the deepest part of the rim syncline [2]. They are, in turn, surrounded by less well-exposed rocks of the Ventersdorp and Transvaal Supergroups.

This study: Mesoscopic shock-related features include shatter cones and (at least some) pseudotachylitic breccias. Pseudotachylitic breccias are ubiquitous in the collar rocks. Most commonly, they are found along bedding planes where they reach centimeters in width and sometimes can be traced for many hundreds of meters, but they also occur oblique and perpendicular to the bedding. The abundance of pseudotachylitic breccia appears to increase towards fault and fold structures, and, in places, is especially prominent in the hinge zones of large-scale (hundreds of meters) folds. Thinly-bedded pelitic sediments typically display pseudotachylitic breccia vein-fracture networks with a fracture spacing of centimeters to a few tens of centimeters. Although evidence of displacement along these veins is generally lacking, in a few cases the veins display en echelon tension gashes as well as displacements of up to several centimeters. Vein thicknesses increase to 10-20 cm along the contacts of the more massive meta-diabase sills (where some meter-wide pods or network breccias have also been observed) and quartzites. In the crystalline rocks in the core of the dome veins and breccias are typically more anastomosing and show a network-like distribution.

Shatter cones are present throughout the collar and show two general orientations: prominent partial cone fractures are commonly found on bedding planes, but random orientations of apices are also observed at numerous localities. The distribution of shatter cones seems to be related to different rock types, as there is a relative abundance of shatter cones in the rocks in the outer parts of the collar, and fine-grained argillitic rocks are preferred strata for intense development of shatter cones and related fractures. More detailed field and sample-based studies of this fracture phenomenon will be carried out in due course.

Results from a large-scale structural investigation of available Landsat images and aerial photos of the study area, as well as from surface mapping of several radial traverses across the Witwatersrand Supergroup show that large-scale features seem to be related to tangential shortening during the formation of the central uplift. The collar of the Vredefort impact structure shows a broadly circular shape on a large-scale view, (although the southern and eastern half of the dome is buried beneath Phanerozoic sediments). However, the collar strata are divided into several polygonal segments arranged at angles of ~30-45° to one-another. The orientation asymmetry in the collar rocks is represented by steeply up- to overturned strata in the northern and northwestern part of the collar and moderate normal dips in the southeastern sector. Recent structural mapping in the Archean gneissic basement in the core of the dome by Lana et al. [3,4,5] has shown differential rotation of the rocks related to doming, with fabrics in the outer parts of the core rotated relative to those in the center. Within the structural domains of the collar, strong evidence for block rotation has been found. The presence of rotated megablocks in the core of the dome, however, cannot be confirmed. Symmetric and asymmetric folding, and associated radial faulting parallel to the fold axial planes affect the collar strata. Large-scale radial faults appear to have sinistral offsets of up to hundreds of meters, however, definitive kinematic indicators are absent. A set of smaller scale transverse faults, which are oriented at an oblique angle to the radial faults, shows both dextral and sinistral displacements, and may represent a conjugate strike-slip set. The folding and faulting

suggest a brittle-ductile response to doming, with the asymmetry of the major structures suggesting an accommodation of the tangential shortening in the manner of an iris-diaphragm. This, in turn, may reflect an originally inclined target sequence as suggested by Lana et al. [6].

On an outcrop-scale, the fracture pattern is complex and can be related to the formation of the central uplift (small-scale subvertical and radial faults), whereas shallowly outwards-dippingjoints are linked to radial and tangential collapse. The dominant set of fractures is a radial set of subvertical joints. This set displays small strike-slip displacements. The second prominent set of joints is parallel to bedding but is listric in places, dipping towards the center of the dome. Slickensides, observed on joint surfaces of this set indicate a normal dip-slip character. In places, the bedding-parallel joints are filled with submillimeter wide pseudotachylitic veins. A shallowly outward-dipping set is consistently present throughout the collar rocks. This trend usually shows a wider spacing than the first two sets (at a dm to m scale), and is only rarely pervasive. The outwards-dipping joints also display striated surfaces and a normal sense of slip, displacing the hanging-wall outwards. Due to the character of the exposures, the slip magnitude is not clear, but it appears to be on the millimeter- to centimeter-scale. The fourth trend of joint is only present locally in the collar and represents an oblique radial joint set dipping at an angle of up to 45° to the subvertical radial joints.

The density of all joint sets increases towards the traces of large-scale faults, however, the large-scale faults are poorly exposed. In general, the intensity of faulting, folding, jointing and pseudotachylite veining decreases radially outwards.

Discussion: Analysis of the initial results from regional and field mapping suggests that the formation of the Vredefort central uplift involved partitioning of strain into radial zones of high strain. At least one of these zones appears to represent a reactivated pre-impact fault. The asymmetry of dips between the northwestern and southeastern sectors of the dome suggest a northwesterly dipping supracrustal sequence prior to the impact. Based on restoration of the pre-impact orientations of the basement fabrics and collar strata, Lana et al. [6] suggested the overturned dips in the NW and normal dips in the SE, resulted from a uniform ~90° rotation of a NW dipping sedimentary sequence. A brittle-ductile deformation regime for the Vredefort impact structure is consistent with observations from experiments by Kenkamnn [7]. Whilst the large-scale features are consistent with tangential shortening associated with the initial formation of the central uplift, most of the small-scale joints appear to be related to radial extension, which most likely occurred during the collapse of the central uplift. The temporal relationships between these features and the large-scale fold-and-thrust features described by Brink et al. [8,9,10] from the outer parts of the rim syncline are, however, not well established, especially as Killick [11] inferred inward-directed extensional collapse along major faults in this region to generate the voluminous pseudotachylitic breccias visible in the goldfields.

The timing of pseudotachylitic breccia development remains enigmatic. In recent studies, Gibson and Reimold [12] and Dressler and Reimold [13] proposed a shock origin for the bulk of the breccias. Given the features observed in the present study, it is possible that shock-generated veins might not have quenched prior to the onset of the crater modification phase and, thus, could have been mobilized into younger fractures. Alternatively, however, some of the breccias may have a non-shock origin, as has been suggested by workers such as Martini [14].

Conclusions: Brittle and ductile structural features in the collar rocks of the Vredefort dome can be related to different stages in the formation of the Vredefort impact structure. Shock-related features include shatter cones and pseudotachylitic breccias. Large- and small-scale subvertical folds and radial and transverse faults appear to be related to the initial formation of the central uplift, with more pervasive fractures linked to subsequent radial and tangential collapse.

References [1] Gibson, R.L. and Reimold, W.U. (2001) Memoir 92, Council for Geoscience, 111pp.; [2] Henkel, H. and Reimold, W.U. (1998) Tectonophys. 287, 1-20; [3] Lana, C. et al. (2000) Geol. Soc. S. Afr., Late Abstracts, 2pp.; [4] Lana, C. et al. (2001) LPSC XXXII, #1032, LPI Houston, 2pp.; [5] Lana et al. (2003), Tectonophys., in press; [6] Lana, C. et al. (2002), submitted to Meteoritics and Planet. Sci.; [7] Kenkmann, T. (2002), Geol. 30, 231-234; [8] Brink, M.C. et al. (1997), Tectonophys. 270, 83-114 ; [9] Brink, M.C. et al. (2000a) J. Afr. Earth Sci. 30, 99-117; [10] Brink, M.C. et al. (2000b) S. Afr. J. Geol. 103, 15-31; [11] Killick, A.M. (1993), PhD Thesis (unpubl.), Rand Afrikaans Univ., Johannesburg, 273pp.; [12] Gibson, R.L. and Reimold, W.U. (2002) Abstract, Transport and Flow Processes in Shear Zones Conf., TSG, London; [13] Dressler, B.O. and Reimold, W.U. (2003), LPSC XXXIV, LPI Houston, in press ; [14] Martini, J.E.J. (1991), Earth. Plan. Sci. Lett. 103, 285-300.

NEW EVIDENCE RELATED TO THE FORMATION OF SHATTER CONES; WITH SPECIAL EMPHASIS ON STRUCTURAL OBSERVATIONS IN THE COLLAR OF THE VREDEFORT DOME, SOUTH AFRICA. F. Wieland, (wielanf@science.pg.wits.ac.za), W.U. Reimold, and R.L. Gibson, Impact Cratering Research Group, School of Geosciences, University of the Witwatersrand, Private Bag 3, P.O. Wits 2050, Johannesburg.

Summary: Shatter cones have been studied for decades without fully resolving their formation. New field observations on shatter cones from the Vredefort Dome give new insight into the formation of this impact deformation phenomenon. The orientations of shatter cone apeces, as observed in the field, are not uniform with regard to the center of the structure, and show a variety of prominent directions: most apex orientations are normal to the strike of the bedding (and parallel to the dip direction of the bedding plane), as well as parallel to the strike (and normal to the dip direction of the bedding plane). No relationship exists between angles of striations, i.e., "protruding bundles of striations" on shatter cone surfaces as defined by Sagy et al. [1], and the distance of sample location from the crater center.

Introduction: The Vredefort dome, the eroded central uplift of the 2.02 Ga, ca. 300 km wide Vredefort impact structure, is a prominent, ~80 km wide, structural and geophysical feature about 120 km SW of Johannesburg. The dome consists of an ~45 km wide core of Archean basement gneisses surrounded by a collar of subvertical/partially overturned Late Archean to Paleoproterozoic supracrustalsstrata. The impact origin of the Vredefort structure is now widely accepted because of extensive bona fide evidence for impact [cf. review by 2]. Shatter cones are abundant throughout the collar strata [3] and also occur in places in the basement granitoids. Despite much field and some laboratory work, the genesis of shatter cones is still not resolved. Early workers emphasized that shatter cones were formed due to the interaction of a shock wave with heterogeneities in target rock, causing scattering, refraction, and reflection of the wave. It w widely accepted that orientations of shatter cone apeces point away from the center of an impact structure, and after rotation of upturned strata, inward towards the explosion center. Nicolayson and Reimold [4] debated this argument and showed that the variety of apex orientations measured at given sites in the collar of the Vredefort Dome is more complex. They also described a distinct relationship between individual shatter cones and so-called multipli- striated joint sets (MSJS), which occur as planar to curviplanar fractures pervasively throughout the Vredefort collar and are also observed in the South range of the Sudbury Structure. These authors concluded that it was not possible to fit all recorded striation orientations from a single site to a single "master" cone. Recently, Sagy et al. [1] suggested a relationship between so-called "striation angles" and distance of the sample from the center of the crater. They defined striations as forming distinctive ridges on the surface of shatter cone segments. The striation angle was defined by the flanks of these ridges. Recent numerical modeling [5] suggests that shock wave reflection caused by "soft" deformations could result in varied orientations of shatter cones.

This study: Samples were collected from and *in-situ* striation orientation measurements performed at a number of sites throughout the northern collar of the Vredefort Dome, extending to about 60 km from the center of the core. These sites occur in different lithological units, all of them belonging to the Witwatersrand, Ventersdorp and Transvaal supergroups. Surfaces of Shatter cones from other impact sites, including Canada and Germany, were also studied. Shatter cones are distributed irregularly throughout the Vredefort collar, with their relative density depending on outcrop accessibility and lithology. Shatter cones have been identified as far north as 65 km from the center of the dome, extending the shatter cone limit given by Therriault et al. [6] by a further 20 km. Generally, only parts of shatter cones are exposed, and complete cones are very rare. The segments are different in size (a few cm to dm) and orientation. Although commonly well developed in fine-grained rocks [4], shatter cones can also be present in massive quartzites. Some of the best exposures of shatter cones are found in the medium-grained Johannesburg and Turffontein quartzites, Upper Witwatersrand Supergroup, in the northern and northwestern part of the collar, and in the Booysens Shale formation exposed along a road-cut in the northwestern sector.

Regarding the orientation of shatter cones, earlier workers suggested a preferred orientation of the apeces downward and outward from the crater center. Taking into account that the strata of the collar have been up- to overturned, rotation of the bedding back to their presumed pre-impact position would result in an orientation of the shatter cone apeces to upward/ inward directions. Recent observations by Nicolayson and Reimold [4], confirmed by the present study, however, indicated a more diverse orientation pattern of shatter cones. Two main cone orientations are observed. The most common one is indeed normal to the strike of the bedding (and within the bedding surface) and would be compatible with the rotation theory. However, the second trend is parallel to the strike of the bedding. Apeces related to both these

trends may point both up- and downward. In places, a third orientation is observed, with apex directions at 30 to almost 60° to the strike of the bedding (trending in different directions, e.g., 300, 30, 130, and 230 degrees for bedding trending at 90/93E). Again, cone apeces of set 3 may also face either upward and /or downward.

The geometry of striations on the surface of shatter cones has also been investigated. Striations have commonly been described as directional and branching radially off the apex. This is the most dominent striation pattern in the Vredefort Dome. In some places, however, subparallel to parallel striations are observed, which has already been emphasized by [3] and [4]. Locally, cone segments show an almost flat surface, with subparallel to parallel striations.

The concept of Sagy et al. [1] was investigated and numerous angles of striation ridges measured on cones from Vredefort and elsewhere. Striation bundles/ridges are epitomized in the horsetailing patterns known from many impact structures and, at Vredefort, best observed at Schoemansdrif bridge. The so-called striation angles vary frombundle to bundle and from cone to cone, and not from site to site. Our findings indicate ranges of angles even on the surface of a single cone segment. Usually the variation is from ~20 to 45°, but angles from 15 to 47° on a single sample have been recorded. The variation of average angle width does not change consistently along a radial traverse through the collar of the Vredefort Dome – in stark contrast to the conclusions of [1].

Discussion: The orientation of shatter cones is more diverse than described in previous studies. We confirm that the most prominent direction of cone apeces in the collar strata is normal to the strike of the bedding (pointing upward and outward). After restoring the pre-impact position of the bedding, these shatter cones would point towards the center of the impact structure. However, there are also other orientations, parallel to the strike of the bedding and oblique to it, which have been disregarded in the past. These two orientations are not restricted to certain parts of the collar; they occur together at some sites, whereas at others only one of them may occur – however, always together with the main tend.

Two different patterns of striations have been observed. Most prominent is the radial appearance of striations on typically conical shatter cone surfaces. The striations branch off the apex and show a strong directionality. Locally, however, and for still unexplained reasons (i.e., no field control for this can be offered), where almost flat shatter cone surfaces have been observed, the striations seem to be subparallel to parallel to each other, making it difficult to determine the orientation of a cone apex. In addition, [3,4] described radial trends of striations as well as subparallel trends from joint-related occurrences. Angles formed by each bundle of striations on ridges on shatter cone surfaces show also strong diversity. The width of these angles varies from site to site throughout the collar and even ranges from tight angles to open ones on the same shatter cone segment.

Conclusion: The model of back-rotation of strata to their pre-impact position does not satisfy the variety of apex orientation data recorded. Shatter cones parallel to bedding would not change their orientation towards the center of the crater by simple back-rotation into likely pre-impact orientations. Complex pre-impact structure can not be invoked either, as again simple back-rotation should still show a consistent behavior for measurements from a given site (up to a few m in extent). Complex post-impact faulting/folding deformation on a macro-scale can also be excluded, for the same reason.. If one subscribes to the premise that the cone apex should always point towards the direction of the energy source, these observations imply a scattering or reflection of the shock wave, while propagating through the target rock. This may have been caused by inhomogeneities in the rock (such as textural or structural [joints, bedding planes] heterogeneities) or change in lithology [e.g., grain size, degree of recrystallization] and mineral content. This concept has recently been supported by numerical modelling of shatter cones by Baratoux and Melosh [5]. Angles defining striation bundles on shatter cone segments show absolutely no evidence of a relationship between the width of such angles and the distance of the sample location from the crater center, as was postulated by [1]. A main problem regarding the nature of shatter cones remains the clearly demonstrated [4] relationship between the MSJS fracturing phenomenon and cone geometry.

References [1] Sagy, A. et al. (2002), Nature 418, 310-313; [2] Gibson, R.L. & Reimold, W.U., CoG, Pretoria, Memoir 92, 111pp.; [3] Manton, W.I. (1965), New York Acad. Sci. Ann. 123, 1017-1049 ; [4] Nicolaysen and Reimold, W.U. (1999), JGR 104, 4911-4030; [5] Baratoux, D. & Melosh, H.J., (2003) 34th LPSC Houston, CD-ROM #1013; [6] Therriault et al. (1997a), MAPS 32, 71-77.

IMPACT MELT ROCKS IN THE "CRETACEOUS MEGABLOCK SEQUENCE" OF DRILL CORE YAXCOPOIL-1, CHICXULUB CRATER, YUCATAN, MEXICO. A. Wittmann[1], T. Kenkmann[1], R.T. Schmitt[1], L. Hecht[1], D. Stöffler[1]. [1]Institut für Mineralogie, Museum für Naturkunde, Humboldt-Universität zu Berlin, Invalidenstr. 43, D-10115 Berlin, Germany, axel.wittmann@rz.hu-berlin.de

Introduction: The Yaxcopoil borehole (Yax-1) penetrates below the impactite units through 600 m of Cretaceous sediments (894.9 m – 1510.9 m). These units are regarded as a displaced "megablock" [1]. This stratified sequence was intruded by suevitic dikes, impact melt dikes and several clastic, polymict dikes. We present preliminary petrographic and geochemical investigations of these dikes.

Suevitic dikes are present at depths of 909, 910 and 916 m with thicknesses of 10 to 130 cm and moderate to steep dipping angles. They are composed of a variegated mixture of clast types including sedimentary (dolomite, limestone, anhydrite), crystalline basement (granitic) and melt fragments. Melt fragments are crystallized and vary in composition and grade of alteration. Table 1 shows whole rock compositions similar to the impactites from a depth of 794 to 894 m if compared to data from [2]. Melt rock fragments show compositions that are well comparable to melt fragment compositions from the overlying impactite units (Hecht, unpublished data). Melt rock types from Table 2 are shown in Figs. 1 and 2. Altered melt rock fragments frequently host shocked mineral fragments like quartz and feldspar displaying multiple sets of PDFs (Fig. 3) or ballen and checkerboard structures. Frequently, mm-thick dike-like structures composed of fine grained carbonate transsect the suevitic dikes sharply. Flow features are present within these structures as bands of congested carbonate and pore fillings with a hydrated Na-silicate (Fig.1). Anhydrite flakes occur in the centre of these structures and thus suggest some type of channelized flow. This carbonate type is in stark contrast to coarsely crystallized calcite in vugs and lenticular pores reminiscent of vesicle shapes in melt fragments.

Impact melt dikes occur at depths of 1347 – 1348 m with thicknesses of 1 to 33 cm and shallow dip angles. The greenish, silicate melt is also present as a minor component in the dolomite breccia units down to a depth of about 1368 m [4]. On a microscopic scale, euhedral dolomite grains form a equigranular fabric with interstitial brown silicate melt which was altered to clay minerals. Few micritic carbonate clasts are present which show features of resorption. Melt also appears as anastomosing veins transsecting the carbonate fabric.

Various brittle faults transsect the fabric and seem to having been active while some melt was still liquid. The close relationship of carbonate and silicate melt suggests that the carbonate component might have been in a molten state during the emplacement of the silicate melt component. Whole rock geochemical data and EMP measurements of sample 1347,96 are presented in Tables 1 and 2. The impact melt rock consists of a mixture of dolomite and a silicate basement component that is different from the component of the impactite units from 794 – 895 m and the suevitic dikes. Most strikingly, Al_2O_3, TiO_2, K_2O are enriched and SiO_2 and CaO are depleted with respect to the silicate melt fragments of the suevite type units above.

Clastic, polymict dikes may possibly also host altered impact melt rock fragments. For a review of these lithologies see [3]. Brown silicate clasts (Fig. 4) are present along with various other clast types. However, strong alteration to potassium feldspar obscures possible primary melt features in these silicate clasts. Whole rock geochemical data is presented in [3] and EMP measurements of silicate clasts from sample 1314,77 is shown in Table 2. These clasts are mainly composed of potassium feldspar and a minor Mg-bearing component, possibly clay minerals which could account for the brownish colour. Pyrite is the carrier of sulfur and iron in these clasts.

Conclusions: Suevitic breccia dikes in YAX-1 show similar compositions and alteration features as the impactite units above. They most closely resemble the lowermost impactite Unit 6 ("Lower Suevite") which is interpreted as ground surged material [2]. This interpretation fits well with a kinematic model of drag and spallation induced delamination [4]. The impact melt rock dikes at 1347-1348 m in YAX-1 have a chemical composition that is distinctly different from the suevitic materials so far known in YAX-1. An impact related origin of the clastic, polymict dikes could be indicated by altered silicate clasts that may be fragments of impact melt rock dikes similar to those from 1347-1348 m. The kinematic implications would allow for that possibility since brittle, impact related fracturing of the impact melt dikes post-dated the emplacement of the melt [4].

References: [1] Kenkmann et al. (2003) Geophys. Res. Abstr. vol. 5, # 5098. [2] Stöffler et al. (2003) LPS XXXIV #1553. [3] Wittmann et al. (2003) LPS XXXIV #1386. [4] Kenkmann et al. 'The Cretaceous sequence of the Chicxulub YAX-1 drillcore: What is impact-derived ?' (2003), this volume.

Acknowledgement: *This work is funded by the German Science Foundation (DFG-grant KE732/8).*

Table 1: Whole rock geochemistry of impactite dikes (d) and neighbouring host rocks (h), XRF analyses, total Fe as Fe_2O_3 and total S as SO_3.

weight-%	910.23 m (d)	910.45 m (d)	910.45 m (hr)	916.34 m (d)	1347.96 m (d)	1348.36 m (hr)
SiO_2	12.4	48.6	1.1	39.2	31.2	1.2
TiO_2	0.17	0.56	<0.01	0.39	0.94	0.03
Al_2O_3	3.56	14.9	0.3	11.7	13.9	0.5
Fe_2O_3	1.03	3.18	1.32	2.63	6.91	0.93
MnO	0.06	0.04	0.02	0.04	0.03	0.01
MgO	0.71	4.21	0.73	4.76	8.28	20.0
CaO	43.4	6.92	53.9	16.4	9.22	31.5
Na_2O	0.30	1.63	<0.02	1.82	0.69	0.08
K_2O	2.88	5.69	0.27	3.97	5.20	0.21
P_2O_5	0.02	0.01	0.01	0.03	0.02	0.01
SO_3	0.8	2.3	1.5	1.5	3.5	0.2
LOI	34.7	11.3	40.8	17.1	19.5	45.3
total	100.03	99.34	99.95	99.54	99.39	99.97

Table 2: EMP data for suevitic dike melt rock clasts (910,45 m and 916,23 m), impact melt rock dikes (1347,96 m) and silicate clasts from clastic, polymict dikes (1314,77 m).

weight-%	910,45 type I	916.23 type II	910.45 type III	916.23 type III	1347.96	1314.77
SiO_2	53.86	56.40	43.69	33.60	47.53	55.55
TiO_2	0.46	0.39	0.01	0.44	1.09	0.71
Al_2O_3	18.97	17.06	5.93	13.30	22.11	18.10
FeO*	3.83	1.61	3.09	3.86	4.69	1.18
MgO	6.14	0.48	22.20	26.11	3.40	1.70
CaO	0.82	3.75	0.88	1.56	0.47	0.57
Na_2O	0.34	3.55	1.82	0.45	0.17	0.23
K_2O	4.91	6.68	0.13	0.08	7.48	11.40
total	89.34	89.95	77.99	79.48	87.29	89.43

* total Fe as FeO

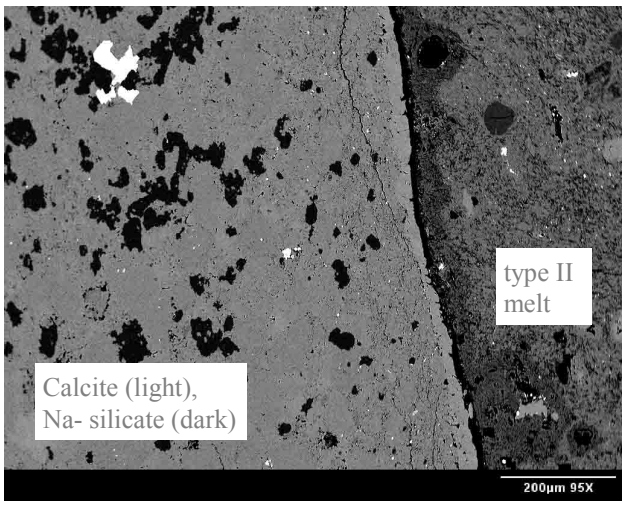

Fig. 1 Melt fragment and carbonate vein in suevitic dike at 916,23 m, BSE image. Melt type relates to Table 2.

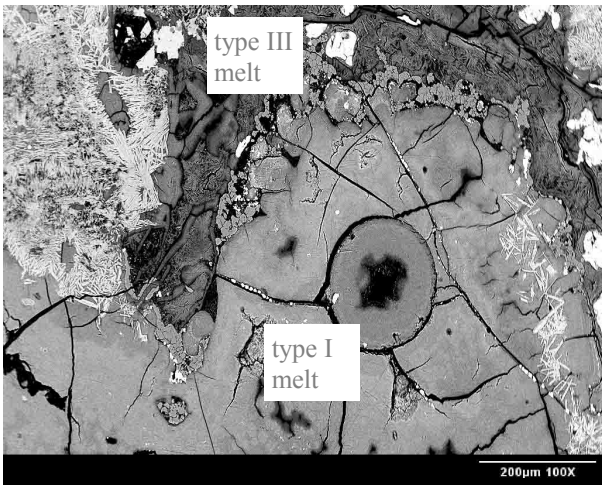

Fig. 2 Melt fragment in suevitic dike at 910,45 m, BSE image. Melt types relate to Table 2.

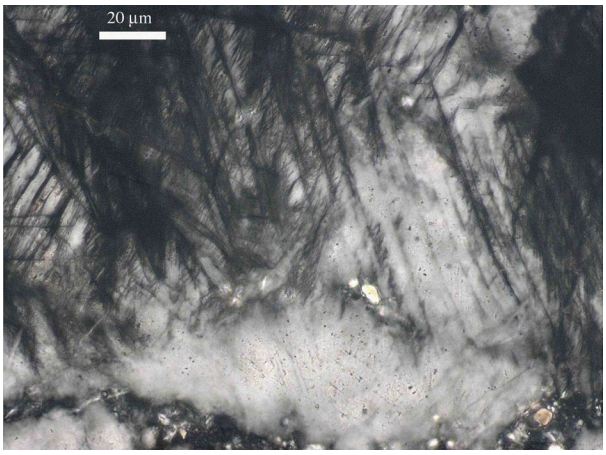

Fig. 3 Dark maskelynite and radiating sets of PDFs in feldspar grain in suevitic dike 909,01 m. Crossed polars photograph.

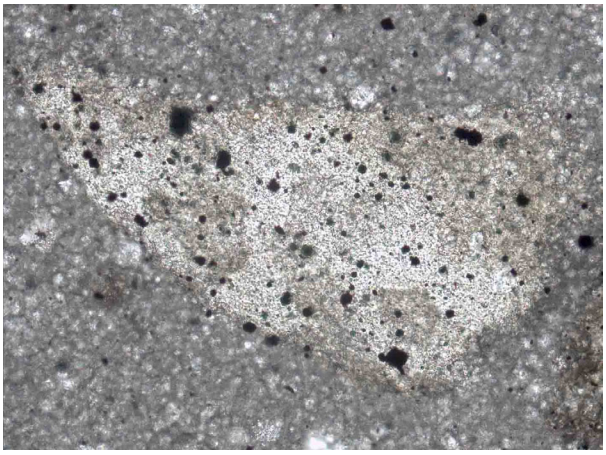

Fig. 4 0.45 mm long, light brown silicate clast in clastic, polymict dike 1314,77 m. Plane polarized light.

NUMERICAL MODELLING OF IMPACT CRATER COLLAPSE UTILISING DIFFERENT CONSTITUTIVE EQUATIONS. K. Wünnemann[1], [1]Department of Earth Science and Engineering, Imperial College London, London SW7 2AZ, United Kingdom (k.wunnemann@ic.ac.uk)

Introduction: Although it is now generally accepted that the heavily cratered landscapes on planets, e.g. the Moon, testify that impact cratering is an important geological process in the evolution of all planetary bodies [1], the process of crater formation itself is still not fully understood.

The observed impact craters fall into two different morphological cases: Simple bowl-shaped craters and the more complex variant with central peaks or rings and flat crater floors. It is generally agreed that both crater forms are the result of a gravity driven modification process of a hemispherically shaped "transient crater". Its size is essentially determined by the kinetic energy of the impactor. If a certain depth of the transient cavity is not exceeded the crater is more or less stable in the gravity field. The cavity remains approximately unchanged and a simple crater arises. In contrast, complex craters are formed if the transient cavity is deeper than the threshold depth or larger than the equivalent diameter. A cavity of this size can no longer resist gravity forces and the crater collapses.

The threshold diameter for the transition between both crater types is a function of 1/g [2]. For the Moon it is 15-20 km, and for the earth 2-4 km, depending on sedimentary or crystalline target composition.

To explain the process of crater formation several numerical models have been proposed, which show [3,4] that the collapse of the transient cavity is mainly controlled by the ratio of material strength Y to the overburden pressure at maximum transient crater depth d_{max} in pure hydrodynamic (strengthless) regime:

$$S = \frac{Y}{\rho g d_{max}} \qquad (1)$$

To match the numerical models with the observed crater morphologies and crater sizes the specific mechanical properties of the target rock in the vicinity of the crater must be assumed to be like the ones of a fluidised media [5]. This means, that a significant, but temporary weakening of target strength is required to explain collapse. The large scale rheology of rock is complex and cannot be reproduced in the laboratory with measurements on small samples. In the present work different kinds of strength models and softening mechanisms are implemented into a modified version [6] of the original SALE hydrocode [7] to assess their effect on crater collapse.

Constitutive Equations: In order to investigate the rather complex mechanical behaviour of rocks under high stress in a large scale process such as crater collapse, different constitutive equations are utilised. For a detailed summary of the different mechanisms that have an effect on strength behaviour see [1]:

Constant Yield Strength: A constant value for the yield strength Y during the entire cratering process is the simplest assumption one can make but it may describe the behaviour of intact consolidated material adequately. A typical value for the strength of most rocks is some 100 MPa.

Mohr Coulomb Model: In this constitutive equation, the shear strength takes on the value of Y_c (the cohesion) at zero confing pressure and increases with pressure p up to a certain limiting value Y_{max}, which is comparable to the Hugoniot Elastic limit. The increasing rate is determined by the dry friction coefficient ϕ. The rocks surrounding the crater cavity are heavily fractured, which suggests a relatively small cohesion (e.g. Y_c=0-1 MPa) and a coefficient of dry friction between 0.8-1.

Thermal Softening: It is well known that increasing temperature has the inverse effect on plastic yielding of the material through reduction of the shear strength. Completely molten material exhibits no resistance against stress and flows plastically. Degradation of strength starts well below the melt temperature T_m, approximately at a temperature T=0.5-0.8 T_m .

Acoustic Fluidisation: Another possible weakening mechanism is caused by strong vibrations of rock fragments surrounding the crater induced by the release from high shock pressure. Under such conditions the material adopts a fluid-like rheology (Bingham rheology) with a viscosity that depends on the wavelength of the vibration (determined by average fragment size) and a cohesive strength that is a function of the vibration amplitude (pressure variation). While vibration decays and amplitude decreases the material loses its fluid-like properties until it freezes and adopts again the classical strength behaviour as described above.

Modelling crater collapse: In order to examine the effect of different strength models on crater collapse we carried out numerical simulations containing different strength descriptions of the target rocks and compared the final crater shape with the crater geometry of the Ries impact crater. In each model the value for the strength Y at depth d_{max} is chosen such that S (Eq. 1) always takes on the same value. The results are shown in Fig. 1. Obviously the simulations containing

the acoustic fluidisation model show the best conformance with the Ries crater morphometry, with respect to the crater diameter and crater depth. Whereas more or less similar results are obtained either assuming (i) a short decay time (T_{dec}=16 s) of the acoustically fluidized heavily fragmented debris surrounding the crater cavity with low viscosity (η=150 MPa s) or assuming (ii) a longer lasting vibration (T_{dec}=44 s) and larger sized fragmented blocks with higher viscosity (η=300 MPa s).

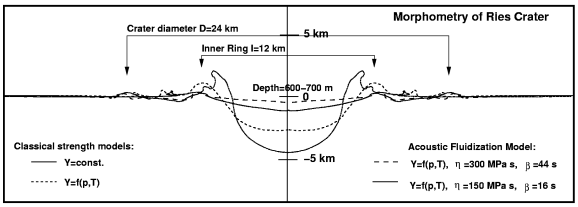

Figure 1: Comparison of final crater shape for numerical models containing different kinds of strength model. Scaling information indicates the diameter (inner ring and outer rim) and depth of the Ries impact crater

Scaling Acoustic Fluidization parameter: Since the fragment size beneath the crater is unknown, one can only find a parameter set for the acoustic fluidisation state (viscosity, decay time) by fitting the observed crater geometry. Although it is obvious that fragment size might differ conspicuously depending on the distance to the point of impact, changes of the average block size at different sized craters [8] suggest that the fragment size and therewith the viscosity may also depend on the size of the crater itself (impact energy). If we assume that larger impactors fragment rocks beneath the crater in larger blocks than smaller projectiles do, suggests, then the acoustic fluidisation parameters can be scaled by the size (energy) of the asteroid. We assume a linear scaling relation between the projectile radius and the viscosity, decay time of the fluidised matter, respectively.

The results are shown in Fig. 2, where the depth-diameter ratio for different sized craters is compared with observed crater geometries [2] on the Moon and Earth. The acoustic fluidization parameters used for the best-fitting curve of the model results are in accordance with the parameter choice given above for the model of the Ries-sized crater on Earth (η=150 MPa s, T_{dec}=16 s).

Conclusion: Crater collapse at the observed threshold diameters on the Moon and Earth can only be explained by some kind of temporary weakening of the strength properties of rocks in the vicinity of the crater. The modelling results of the Ries crater show that the usage of the acoustic fluidisation model leads to the best accordance with the observed crater morphometry. Furthermore, scaling the acoustic fluidisation parameters with respect to the projectile radius allows us to model the crater collapse at the observed threshold diameters between simple and complex crater structures on the Moon and Earth. However, some further improvements of the model are required to meet the usual request of reproducing not only depth-diameter ratios, but the exact morphology of visible natural craters. For instance, this includes the introduction of a spatial variation of fragment size as a function of distance from the point of impact, and further, the analysis of geophysical exploration data of large impact structures to establish how rock properties beneath impact structures vary with crater size.

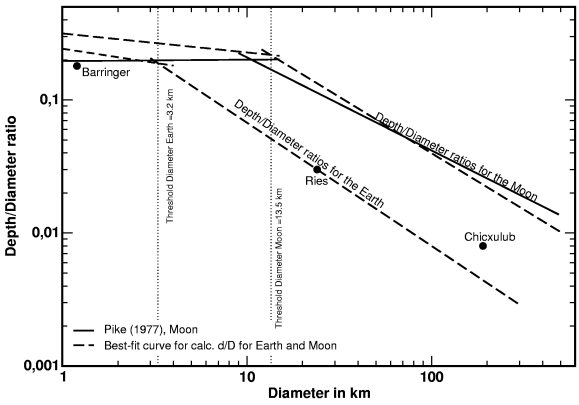

Figure. 2: Depth-diameter ratios versus crater diameter on the Moon and Earth. For comparison, the best-fit curve of observed crater geometries on the Moon taken from [2], and 3 ratios of terrestrial craters (Barringer, Ries and Chicxulub), are also shown.

References:

[1] Melosh H. J., Ivanov B. A. (1999), Annu. Re. Earth Plant. Sci., 27, 385-415. [2] Pike R. J. (1988), In: Mercury, University of Arizona Press, Tucson, 165-273. [3] O'Keefe J. D., Ahrens T. J. (1999), JGR, 104, 27091-27104. [4] Wünnemann K., Ivanov B. A., Lange M. A. (2002) *LPS XXXIII,* Abstract #1277. [5] Melosh H. J. (1989), Impact cratering: A geological process, Oxford University Press, New York, 245 pp. [6] Wünnemann K., Lange M. A. (2002) *DSR II, 49, 969-981.* [7] Amsden A. et al. (1980), Los Alamos National Laboratory Report LA-8095, Los Alamos, 101pp. [8] Kocharyan G. G., Kostuchenko V. N., Ivanov B. A. (1996) *LPS XXVI,* 677-678.

VAALBARA AND TECTONIC EFFECTS OF A MEGA IMPACT IN THE EARLY ARCHEAN 3470 Ma

T.E. Zegers and A. Ocampo

European Space Agency, ESTEC, SCI-SB, Keplerlaan 1, 2201 AZ Noordwijk, tzegers@rssd.esa.int

Abstract
The oldest impact related layer recognized on Earth occur in greenstone sequences of the Kaapvaal (South Africa) and Pilbara (Australia) Craton, and have been dated at ca. 3470 Ma (Byerly et al., 2002). The simultaneous occurrence of impact layers now geographically widely separated have been taken to indicate that this was a worldwide phenomena, suggesting a very large impact: 10 to 100 times more massive than the Cretaceous-Tertiary event.
However, the remarkable lithostratigraphic and chronostratigraphic similarities between the Pilbara and Kaapvaal Craton have been noted previously for the period between 3.5 and 2.7 Ga (Cheney et al., 1988). Paleomagnetic data from two ultramafic complexes in the Pilbara and Kaapvaal Craton showed that at 2.87 Ga the two cratons could have been part of one larger supercontinent called **Vaalbara**.

New Paleomagnetic results from the older greenstone sequences (3.5 to 3.2 Ga) in the Pilbara and Kaapvaal Craton will be presented. The constructed apparent polar wander path for the two cratons shows remarkable similarities and overlap to a large extent. This suggests that the two cratons were joined for a considerable time during the Archean. Therefore, the coeval impact layers in the two cratons at 3.47 Ga do not necessarily suggest a worldwide phenomena on the present scale of separation of the two cratons.

Although the impact 3470 Ma impact may have been more limited in size than previously thought, it is interesting to test if geological events described for the Pilbara and Kaapvaal Craton may represent the structural and magmatic results of an impact. The time series correlation between Lunar and Earth impact history and periods of high volcanic activity (Abbott and Isley, 2002) suggest that there is a causal relationship between crustal growth and meteorite impacts. The era between 3490 and 3400 Ma represents one of the best documented periods in which felsic continental crust was formed by intrusion and extrusion of TTG (tonalite, trondhjemite, granodiorite) melt. The stratigraphy consists almost entirely of mafic to ultramafic volcanic rocks and minor felsic (TTG) volcanic rocks. In this stratigraphy it may not be possible to distinguish impact melts from normal volcanic rocks. In both the Pilbara and Kaapvaal Craton extensional faults have been described, which were active at ca. 3470 Ma, during felsic volcanism and broadly coeval with the impact layers (Zegers et al., 1996, Nijman et al., 1998). These extensional structures have been interpreted as the result of caldera collapse (Nijman et al., 1998, Van Kranendonk et al, 2002) or as the result of delamination of lower crustal eclogite (Zegers and Van Keken, 2001). The question remains if there is any evidence in the geological record that this magmatic event could have been triggered

by meteorite impacts. We will examine the possibility that these extensional fault patterns represent multi ring faults associated with a large impact.

The early Archean greenstone terrains can be regarded as the closest analogue to Martian geology. Therefore the study of impact features in the Pilbara Craton may have implications for understanding impact features on Mars.

References:

Abbott, D.H., and A.E. Isley, 2002, Extraterrestrial influences on mantle plume activity, *Earth and Planetary Science Letters*, v. 205, p.53-62.

Byerly, G.R., D.R. .Lowe, J.L. Wooden, and X. Xie, 2002, An Archaean impact layer from the Pilbara and Kaapvaal Cratons. *Nature*, v. 297, p.1325-1327.

Cheney, E.S., C. Roering, E. Stettler, 1988, Vaalbara (Extended abstract). *Geol. Soc. S. Afr. Geocongr.* v.88, p.85-88.

Nijman, W., B.A. Willigers, and A. Krikke, 1998, Tensile and compressive growth structures: relationships between sedimentation, deformation and granite intrusion in the Coppin Gap Greenstone Belt, eastern Pilbara, Western Australia. *Precambrian Research*, v. 88, p.83-108.

Van Kranendonk M. J., A. H. Hickman, R. H. Smithies, D. R. Nelson, and G. Pike, 2002, Geology and Tectonic Evolution of the Archean North Pilbara Terrain, Pilbara Craton, Western Australia. *Economic Geology Bulletin*, V. 97, p. 695-732.

Zegers, T.E., S.H. White, M. de Keijzer, and P. Dirks, 1996, Extensional structures during deposition of the 3460 Ma Warrawoona Group in the eastern Pilbara Craton, western Australia. *Precambrian Research*, v.80, p.89-105

Zegers, T.E. and P.E. van Keken, 2001, Middle Archean continent formation by crustal delamination. *Geology*, v.29, p.1083-1086.